The methyl phosphate capping enzyme Bin3 is a stable component of the fission yeast telomerase holoenzyme

Jennifer Porat[1], Moaine El Baidouri[2,3], Jorg Grigull[4], Jean-Marc Deragon[2,3,5], & Mark A. Bayfield[1*]

1. Department of Biology, York University, Toronto, Canada

2. LGDP-UMR5096, Université de Perpignan Via Domitia, Perpignan, France

3. CNRS LGDP-UMR5096, Perpignan, France

4. Department of Mathematics and Statistics, York University, Toronto, Canada

5. Institut Universitaire de France, Paris, France

*Correspondence: bayfield@yorku.ca (M.A.B.)

Abstract:

The telomerase holoenzyme is critical for maintaining eukaryotic genome integrity. In addition to a reverse transcriptase and an RNA template, telomerase contains additional proteins that protect the telomerase RNA and promote holoenzyme assembly. Here we report that the methyl phosphate capping enzyme (MePCE) Bin3 is a stable component of the *S. pombe* telomerase holoenzyme. Bin3 associates with the telomerase holoenzyme and U6 snRNA through an interaction with the recently described LARP7 family member Pof8, and we demonstrate that these two factors are evolutionarily linked in fungi. Our data suggest that the association of Bin3 with telomerase is independent of its methyltransferase activity, but rather that Bin3 functions in telomerase holoenzyme assembly by promoting TER1 accumulation and

24 Pof8 recruitment to TER1. Taken together, this work yields new insight into the composition,
25 assembly, and regulation of the telomerase holoenzyme in fission yeast as well as the breadth
26 of its evolutionary conservation.
27
28 **Introduction:**
29 To ensure complete DNA replication, the termini of eukaryotic chromosomes contain tandem
30 repeats, or telomeres, that can be continually extended as the ends of linear chromosomes are
31 lost through DNA replication[1]. Telomeres serve as protection from DNA degradation, end-to-
32 end fusions, chromosomal rearrangements, and chromosome loss [1,2]. With very few exceptions,
33 eukaryotes extend telomeric DNA sequences through the telomerase holoenzyme, a complex
34 containing the telomerase reverse transcriptase (Trt1 in the fission yeast *Schizosaccharomyces*
35 *pombe*), an RNA template (TER1 in *S. pombe*), and accessory proteins that promote complex
36 assembly and tethering to telomeric DNA [1–5]. While the reverse transcriptase/RNA template
37 core of telomerase is generally well-conserved among eukaryotes, major differences exist,
38 including in the sequence and structure of the RNA template. In contrast to ciliate telomerase
39 RNAs, which are small RNA Polymerase III transcripts [6], yeast and metazoan telomerase RNAs
40 are longer and transcribed by RNA Polymerase II as precursors[7,8]. These precursors then
41 undergo an extensive maturation process to yield the mature form that integrates into the
42 telomerase holoenzyme [3,4,7,8].
43
44 In *S. pombe,* the mature form of TER1 is generated from an intron-containing precursor through
45 a spliceosome-catalyzed reaction involving release of the 5' exon prior to exon ligation [9]. TER1

46 maturation then proceeds with the sequential binding of the Sm and Lsm complexes. Sm
47 proteins, well-characterized for their role in splicing, bind TER1 immediately upstream the 5'
48 splice site and promote 3' maturation and the addition of a 5' trimethylguanosine (TMG) cap by
49 the methyltransferase Tgs1 [10]. The Sm complex is then replaced by the Lsm2-8 complex, which
50 serves to protect the mature 3' end of TER1 from exonucleolytic degradation and promotes the
51 interaction between TER1 and Trt1 in the active telomerase holoenzyme. The switch from the
52 Sm to Lsm complexes correlates with distinct, non-overlapping substrates: TER1 precursors are
53 exclusively bound by the Sm complex, while the mature form of TER1, ending in a polyuridylate
54 stretch upstream the spliceosomal cleavage site, is only bound by the Lsm2-8 complex [10].
55
56 More recently, a role has been proposed for Pof8, a La-related protein 7 (LARP7) homolog, in
57 telomerase assembly and telomere maintenance in *S. pombe*. Ciliate LARP7 family proteins,
58 including p65 from *Tetrahymena thermophila*, have previously been characterized for their
59 functions in telomerase assembly [11]. Binding of p65 to stem IV of the *T. thermophila* telomerase
60 RNA TER results in a conformational change to the RNA and subsequent binding of the reverse
61 transcriptase TERT, suggesting a p65-dependent hierarchical assembly of the telomerase
62 holoenzyme [12]. Pof8 is hypothesized to function similarly in *S. pombe*, with Pof8 binding to TER1
63 promoting recruitment of the Lsm2-8 complex and enhancing the interaction between TER1
64 and Trt1. Accordingly, Pof8 deletion strains possess shorter telomeres indicative of a defect in
65 telomerase function [13–15]. Pof8 also functions in telomerase RNA quality control through
66 recognition of the correctly folded pseudoknot region and subsequent recruitment of the Lsm2-
67 8 complex to protect the 3' end from degradation [16]. Telomerase-related functions in LARP7

68 family proteins, particularly Pof8, map to a conserved C-terminal domain characteristic of
69 LARP7 family members, the extended RNA recognition motif (xRRM)[17,18]. The Pof8 xRRM is a
70 major determinant for Pof8-mediated telomerase activity, contributing to TER1 binding and
71 complex assembly [14,19]. As other fungal Pof8 homologs also possess an xRRM, it is anticipated
72 that Pof8 may have a conserved role in telomere maintenance beyond fission yeast [14,20].
73
74 Conversely, LARP7 homologs in higher eukaryotes are best characterized in the transcriptional
75 regulatory 7SK snRNP, which includes the RNA polymerase III transcribed 7SK snRNA, the
76 methyl phosphate capping enzyme (MePCE), and hexamethylene bisacetamide-inducible
77 protein (HEXIM1/2). The 7SK snRNP inhibits transcription by sequestering positive transcription
78 elongation factor (P-TEFb) and preventing it from phosphorylating the C-terminal domain of the
79 largest subunit of RNA Polymerase II, which is associated with the transition into productive
80 transcription elongation [21–23]. The La module and xRRM of LARP7 bind 7SK through its
81 polyuridylate trailer and the 3' hairpin, respectively, and promote MePCE recruitment to the
82 complex [24,25]. In addition to adding a γ-monomethyl phosphate cap (i.e. CH_3-pppN) to 7SK
83 snRNA as a means of protecting it from 5' exonucleolytic degradation, MePCE remains stably
84 bound to 7SK snRNA to stabilize the complex [24]. MePCE, a homolog of the *Drosophila*
85 *melanogaster* Bin3/BCDIN3 protein, also catalyzes the addition of this atypical cap structure to
86 U6 snRNA [26]. Bin3/MePCE homologs are present in many eukaryotes, but to date little has been
87 studied outside of humans and *Drosophila* [27]. More recent work has identified BCIND3D, a
88 related Bin3 family protein overexpressed in breast cancer cells, as the enzyme responsible for
89 methylating the 5' monophosphate of histidine transfer RNA and pre-miR-145 [28,29]. Despite the

90 many insights into the role of Bin3/MePCE in RNA processing in higher eukaryotes, the function
91 of the *S. pombe* Bin3 homolog has yet to be determined.
92
93 In this work, we have explored the RNA targets of the *S. pombe* Bin3 homolog in an effort to
94 uncover its function. In addition to an expected association of Bin3 with U6 snRNA, we present
95 data showing that Bin3 is a stable component of the *S. pombe* telomerase RNP. Our results also
96 provide evidence for an evolutionarily conserved interaction between Bin3 and LARP7
97 homologs. Importantly, we show that the Bin3-Pof8 interaction is required for the recruitment
98 of Bin3 to both U6 snRNA and the active telomerase holoenzyme. Additionally, we provide data
99 that Bin3 does not catalyze the addition of a γ-monomethyl phosphate cap on TER1, suggesting
100 a catalytic independent function. Rather, we present evidence that Bin3 functions in concert
101 with Pof8 to promote telomerase assembly and TER1 accumulation. Taken together, our results
102 identify Bin3 as a novel component of the *S. pombe* telomerase holoenzyme, thus adding a new
103 layer of complexity to telomerase assembly and telomere maintenance.
104
105 **Results:**
106 ***S. pombe* Bin3 interacts with U6 snRNA and the telomerase RNA TER1**
107 While Bin3/MePCE is conserved in many eukaryotes, its presence in the fission yeast *S. pombe*,
108 an organism lacking 7SK snRNA [27,30], is not well understood. Unlike the longer Bin3/MePCE
109 homologs from higher eukaryotes, *S. pombe* Bin3 only contains a conserved
110 methyltransferase/SAM-binding domain (Figure S1A). Alignment of the methyltransferase
111 domain of *S. pombe* Bin3 to that of *H. sapiens* MePCE and *D. melanogaster* Bin3 reveals that

112 previously identified residues critical for SAM and SAH binding and nucleotide binding [31] are
113 highly conserved in *S.* pombe (Figure S1B,C).
114
115 We first sought to determine the RNA substrates of *S. pombe* Bin3 to better understand its role
116 in the processing of fission yeast non-coding RNA(s). Following integration of a protein A (PrA)
117 tag into the Bin3 genomic locus, we performed RIP-Seq, followed by validation of potential
118 candidate substrates with northern blotting and semi-quantitative RT-PCR (Figure 1, Table S1).
119 Consistent with previous reports of MePCE interacting with U6 snRNA [26], U6 emerged as one of
120 the most highly enriched Bin3-interacting RNA transcripts in our Seq dataset (Figure 1A, Table
121 S1). *S. pombe* U6 is an unusual transcript in that it is transcribed by RNA Polymerase III yet
122 contains an mRNA-type intron removed by the spliceosome [32,33]. Alignment of RIP-Seq reads to
123 the *S. pombe* genome suggested that Bin3 interacts exclusively with the spliced form of U6. We
124 confirmed this with northern blotting, demonstrating robust immunoprecipitation of mature
125 U6 and no immunoprecipitation of the intron-containing precursor (Figure 1B). Chromatin
126 immunoprecipitation studies suggest that 7SK and U6 snRNA may be co-transcriptionally
127 modified by the human MePCE homolog [34], however our data are consistent with a model
128 wherein *S. pombe* Bin3 interacts with U6 post-splicing.
129
130 Surprisingly, the *S. pombe* telomerase RNA TER1 was the most highly enriched hit in the Bin3
131 immunoprecipitates (Figure 1A, C). Given the previously established link between the human
132 Bin3 homolog MePCE and human LARP7, [23] as well as the established link between the *S.*
133 *pombe* LARP7 homolog Pof8 and the telomerase holoenzyme [13–15], we considered the

134 possibility that Bin3 may also be part of the telomerase holoenzyme through an evolutionarily
135 conserved interaction with LARP7 family members.
136
137 **Bin3 interacts with the mature form of TER1**
138
139 Since TER1 processing and maturation involves a spliceosome-catalyzed reaction [9], we next set
140 out to determine the processing state of Bin3-associated TER1 by sequencing the 5' and 3' ends
141 through circularized rapid amplification of cDNA ends (cRACE) (Figure 2A). We also performed
142 cRACE on TER1 immunoprecipitated by Pof8, the telomerase reverse transcriptase Trt1, and
143 Lsm3, all known components of the mature TER1-containing active telomerase holoenzyme
144 [3,4,10,13–15]. All sequenced candidates had a discrete 5' end consistent with the reported 5' end [3,4]
145 and a similar distribution of 3' ends ending immediately upstream the 5' splice site [9], suggesting
146 that Bin3 interacts with the full-length, 3' end-matured TER1 associated with the active
147 telomerase holoenzyme. The heterogeneity observed at the 3' end of all candidates is likely the
148 result of exonucleolytic nibbling prior to binding of the Lsm2-8 complex [10]. To investigate this
149 further, we subjected TER1 RNA immunoprecipitated by Bin3, Trt1, Pof8 and Lsm3 to RNase H
150 cleavage to generate shorter 5' and 3' fragments and compared fragment size by northern blot
151 (Figure 2B). The sizes of the 5' and 3' ends of TER1 were similar across immunoprecipitates,
152 further substantiating that Bin3 binds the mature form of TER1, rather than the intron-
153 containing precursor.
154

155 Further TER1 processing in *S. pombe* involves the addition of a 5' trimethylguanosine (TMG) cap
156 by Tgs1 [10]. Since Bin3 homologs are normally associated with the formation of a γ-monomethyl
157 phosphate cap, and to further understand when Bin3 interacts with TER1 with respect to TER1
158 processing, we examined the cap structure of Bin3-associated TER1 by immunoprecipitating
159 RNA associated with Bin3 and subsequently re-immunoprecipitating this RNA with an anti-TMG
160 antibody. The specificity of the anti-TMG antibody was confirmed by showing that it effectively
161 enriched the TMG cap-containing U5 snRNA over the TMG cap-lacking U6 snRNA or an
162 unrelated tRNA (Figure 2C). While Bin3-associated U6 snRNA was not immunoprecipitated by
163 the anti-TMG antibody, in agreement with data demonstrating the presence of a γ-monomethyl
164 phosphate cap on U6 *in S. pombe* [35], Bin3-associated TER1 RNA was effectively enriched by anti-
165 TMG immunoprecipitation (Figure 2D). These data are consistent with previous work
166 demonstrating a TMG cap on TER1 in *S. pombe,* and also with Bin3 associating with TER1
167 following spliceosomeal cleavage and 5' TMG capping, similar to what has been posited for
168 Pof8 [13]. This suggests that Bin3 interacts with the primary cohort of TMG capped TER1
169 transcripts, and that TER1 is not a substrate for Bin3-catalyzed γ-monomethyl phosphate
170 capping.
171
172 **Bin3 interacts with components of the mature telomerase holoenzyme**
173 Since our results indicate that Bin3 interacts with the mature form of TER1, we set out to
174 confirm the presence of Bin3 in the *S. pombe* telomerase holoenzyme. We immunoprecipitated
175 Bin3 and identified interacting proteins through mass spectrometry, followed by validation
176 using co-immunoprecipitation (Figure 3). We identified Pof8, the Lsm2-8 complex, and Trt1 in

177 Bin3 immunoprecipitates, all of which make up the catalytically active core telomerase
178 holoenzyme [5,10,13–15,36,37] (Table S2). We also detected the RNase P and RNase MRP subunit
179 Pop100 in Bin3 immunoprecipitations. Pop1, Pop6, and Pop7, subunits of RNase P and RNase
180 MRP in budding yeast, have recently been identified as components of the budding yeast
181 telomerase complex [38–40], suggesting that the involvement of RNase P and RNase MRP subunits
182 in telomere maintenance is evolutionarily conserved. The finding that Bin3 interacts with core
183 components of the telomerase holoenzyme, and not the Sm complex nor the TMG capping
184 enzyme Tgs1, suggests Bin3 does indeed associate with the active telomerase holoenzyme
185 rather than a precursor. The involvement of Bin3 in the telomerase holoenzyme was further
186 substantiated by gene ontology analysis to determine overrepresented biological processes and
187 cellular components among the top 50 Bin3 interactors. Telomerase holoenzyme complex
188 assembly and telomere maintenance via telomerase emerged as the top overrepresented
189 biological processes (Figure 3A). Similarly, overrepresented cellular components include the
190 Lsm2-8 complex, the telomerase holoenzyme, and spliceosomal snRNPs (Table S3). We also
191 repeated immunoprecipitations in the presence of benzonase to determine if these interactions
192 are direct or mediated through a nucleic acid intermediate. With the exception of Pof8 and an
193 uncharacterized protein (SPCC18B5.09c), interactions between Bin3 and other components of
194 the telomerase holoenzyme were lost, suggestive of an interaction mediated by TER1.
195
196 We validated the interactions between Bin3 and Pof8, as well as Bin3 and Trt1, through co-
197 immunoprecipitation (Figures 3B, 3C, S2). We also performed co-immunoprecipitations with
198 benzonase, demonstrating that the interaction between Bin3 and Pof8 persists with benzonase

199 treatment, while the Bin3-Trt1 interaction is lost (Figures 3B and 3C). To confirm that the Bin3-
200 Trt1 interaction is mediated by TER1, we repeated co-immunoprecipitations in a TER1 knockout
201 strain. The direct interaction between Bin3 and Pof8 remained intact in the absence of TER1,
202 while the Bin3-Trt1 interaction was completely lost, indicative of Bin3 assembly in the
203 telomerase holoenzyme nucleated, in large part, by the telomerase RNA itself. The RNA-
204 dependence of the interaction between Bin3 and Trt1 is reminiscent both of the budding yeast
205 telomerase RNA TLC1, which acts as a scaffold for telomerase holoenzyme assembly [41], as well
206 as the MePCE/Bin3-containing 7SK snRNP [42]. The finding that Bin3 and Pof8 interact directly is
207 in agreement with previous reports demonstrating a protein-protein interaction between
208 MePCE and LARP7 in the context of the vertebrate 7SK snRNP [34,42], suggesting the direct
209 interaction may be evolutionarily conserved.
210
211 **Bin3 is recruited to the active telomerase holoenzyme through the LARP7 family protein Pof8**
212 We then tested whether Bin3 was recruited to the telomerase holoenzyme through its
213 interaction with Pof8, much like the human LARP7 homolog promotes MePCE recruitment to
214 7SK snRNA [24]. Immunoprecipitation of Bin3 in the context of a *pof8Δ* strain resulted in a
215 complete loss of TER1 binding, providing evidence that the interaction between Bin3 and TER1
216 is dependent on an interaction between Bin3 and Pof8 (Figure 4A,B). Unexpectedly, the
217 interaction between Bin3 and U6 was also lost in the *pof8Δ* strain. Recent findings indicate that
218 mammalian LARP7 binds U6 to guide post-transcriptional modification [43,44], so it is tempting to
219 speculate that Pof8 may also mediate Bin3 binding to U6 in fission yeast. To address this, we
220 immunoprecipitated Pof8 alongside Bin3 and other components of the telomerase holoenzyme

221 and looked for U6 enrichment. We observed slight enrichment of U6 in Pof8-myc
222 immunoprecipitates relative to immunoprecipitation using an untagged strain or the Trt1-myc
223 tagged strain (Figure 4C). We did not see enrichment for the intron-containing precursor,
224 suggesting that like Bin3, Pof8 interacts with the spliced form of U6. The slight enrichment of
225 U6 with Pof8 immunoprecipitation, compared to the more robust immunoprecipitation seen
226 with Bin3 and Lsm3, suggests that Pof8 may transiently bind U6, perhaps serving to load Bin3
227 on U6. Since LARP7 binding has been reported to disrupt the catalytic activity of MePCE [34], a
228 transient Pof8-U6 interaction may be consistent with U6 receiving a γ-monomethyl phosphate
229 cap, compared to TER1, where stable Pof8 binding may prevent Bin3 catalytic activity.
230
231 To further investigate how the presence of Bin3 in the TER1-containing telomerase holoenzyme
232 is reliant on Pof8, we fractionated lysates from wild type and Pof8 knockout strains on a
233 glycerol gradient and analyzed the sedimentation patterns of Bin3, Pof8, TER1, and U6 (Figure
234 S3). We found that Bin3 and Pof8 co-sedimented with TER1 in higher molecular weight
235 fractions in a wild-type strain, as well as in lighter molecular weight fractions that contained U6
236 (U6 present in higher molecular weight fractions likely corresponds to U6 within the
237 spliceosome). In contrast, Bin3 was depleted from higher molecular weight fractions containing
238 TER1 in the absence of Pof8. We also noted a slight shift in TER1 towards lighter fractions in the
239 Pof8 deletion strain, which could be due to a lighter-migrating telomerase holoenzyme lacking
240 Bin3 and Pof8. These data are also consistent with Bin3 stably associating with the telomerase
241 holoenzyme in a manner that is dependent on Pof8.
242

243

244 Knowing that Bin3 interacts with TER1 and components of the telomerase holoenzyme, we next
245 set out to confirm whether Bin3 is part of the catalytically active telomerase holoenzyme. We
246 performed a previously described *in vitro* telomerase assay that relies on the presence of the
247 TER1- and Trt1-containing telomerase holoenzyme to extend an oligonucleotide resembling
248 telomeric DNA [13]. Bin3 immunoprecipitates extended the oligonucleotide in a similar manner
249 previously demonstrated for Pof8 ([13] and see Figure 5D), as well as showed the same loss of
250 activity upon RNase A treatment, supporting the idea that Bin3, much like Pof8, is a component
251 of the active telomerase holoenzyme (Figure 4D). Consistent with previous results[13,16], we also
252 observed a loss of activity for Bin3 immunoprecipitated from a *pof8Δ* strain, which can largely
253 be attributed to the loss of functional, correctly assembled telomerase occurring in the absence
254 of Pof8. Since Trt1 is only recruited to the telomerase holoenzyme following Pof8 and Lsm2-8
255 binding, coupled with the idea that the assay relies on the presence of a reverse transcriptase,
256 these results are consistent with a model in which Bin3 is recruited to TER1 through its
257 interaction with Pof8 and remains bound through subsequent holoenzyme assembly and the
258 catalytic cycle (Figure 4E).

259

260 To further investigate the link between Bin3 and Pof8 in telomerase holoenzyme assembly, we
261 tested whether overexpression of Bin3 could rescue the short telomere phenotype of a *pof8Δ*
262 strain [13–15]. Consistent with a model in which Bin3 requires Pof8 for its assembly into the active
263 telomerase holoenzyme, Bin3 overexpression in a *pof8Δ* strain was insufficient to rescue
264 telomere shortening, as measured by Southern blot, as well chromosome fusions occurring

265 after telomeres reach a critically short length previously associated with *the pof8Δ* strain [13]

266 (Figure S4).

267

268 **Bin3 promotes TER1 accumulation and Pof8 recruitment to telomerase**

269 We then interrogated the functional role of Bin3 in telomerase by creating a Bin3 knockout

270 strain where we replaced the Bin3 open reading frame with a phleomycin resistance cassette

271 which was confirmed by PCR and sequencing, as well as qRT-PCR to confirm a lack of Bin3

272 mRNA (Figure S5A, B). To address conflicting reports in the literature as to the nature of Bin3's

273 essentiality in *S. pombe*[45,46], we back-crossed our Bin3 deletion strain with a wild type strain.

274 Sporulation and tetrad dissections yielded viable haploid colonies possessing phleomycin

275 resistance (Figure S5C), confirming that Bin3 is not essential and enabling us to conduct further

276 mechanistic studies.

277

278 Consistent with its strong dependence on Pof8 for recruitment to telomerase, Bin3 deletion

279 appears to decrease steady-state TER1 levels, much like a Pof8 deletion strain, with no

280 reduction in U6 abundance (Figure 5A). Importantly, re-introduction of plasmid expressed Bin3

281 to *bin3Δ* cells was sufficient to restore wild type levels of TER1 (Figure S5D). To understand the

282 mechanism by which Bin3 appears to promote TER1 accumulation, we combined our Bin3

283 deletion strain with deletion of Rrp6, an exonuclease component of the nuclear exosome that

284 has been previously implicated in TER1 degradation [13,15,16,47,48]. We observed a restoration of

285 TER1 levels in the *bin3Δ rrp6Δ* strain (Figure 5A), similar to what has been observed for Pof8,

286 where Rrp6 deletion rescues decreased TER1 levels[15]. From this, we hypothesize that Bin3

287 promotes TER1 accumulation by preventing 3' decay by the exosome to maintain steady state
288 TER1 levels.
289
290 In line with decreased TER1 levels, Bin3 deletion resulted in shorter telomere length compared
291 to a wild-type strain, which became more evident when genomic DNA was digested with ApaI
292 to yield shorter telomere fragments (Figure 5B). We continued passaging strains to get to the
293 point of crisis (>100 generations), where telomeres are lost and cells either die or circularize
294 their chromosomes, leading to a loss of an observable telomere signal by southern blot [49]. As
295 expected, a strain lacking TER1 showed a complete loss of telomeric DNA, whereas deletion of
296 Pof8 and Bin3 only resulted in shorter telomeres, suggesting that while the two proteins are
297 important for telomere maintenance, they are not strictly required like TER1 (Figure S6).
298
299 To better understand how Bin3 affects telomere length and TER1 accumulation, we examined
300 how the Pof8-TER1 interaction changes upon Bin3 deletion. Somewhat surprisingly, considering
301 that Bin3 completely relies on Pof8 for recruitment to telomerase, we found that Bin3 deletion
302 also impaired Pof8 binding to TER1 (Figure 5C), much like the cooperative binding of Pof8 and
303 Lsm2-8 to TER1 [16]. Similarly, we observed decreased telomerase activity immunoprecipitated
304 by Pof8 in the Bin3 knockout strain, with normalization of the intensity of the extension bands
305 to TER1 levels revealing that the compromised activity cannot only be attributed to the loss of
306 TER1 following Bin3 deletion (Figure 5D, E). Conversely, normalization of telomere extension
307 activity to the amount of TER1 immunoprecipitated by Pof8 revealed that although less Pof8-
308 containing telomerase complexes form in the absence of Bin3, the ones that do form are fully

309 functional (Figure 5D, F). Thus it appears that not only does Bin3 affect TER1 accumulation but
310 also contributes to Pof8 association with TER1, suggesting a further role for Bin3 in ensuring
311 holoenzyme functionality.
312
313 **Pof8-like proteins are associated with Bin3-like proteins in diverse fungal lineages**
314 The interaction between Bin3 and Pof8, coupled with the conservation of such an interaction in
315 other examined eukaryotes, led us to wonder at the extent of this interaction on a phylogenetic
316 scale. While Bin3/MePCE and LARP7/Pof8 family members are ubiquitous in higher eukaryotes,
317 their absence or presence is more varied in fungal lineages. We queried hundreds of
318 representative fungal species for the presence of Bin3- and Pof8-like proteins and identified
319 many species with a) both a Bin3 and Pof8 homolog, b) only a Bin3 homolog, or c) neither a
320 Bin3 nor a Pof8 homolog (Figure 6, S7). Conversely, only four out of 472 examined species
321 contained a Pof8-like protein but no Bin3-like protein, and in these species the Pof8 homolog
322 was noted to have a shortened N-terminal domain that would lack the La module observed in
323 other LARP7 family members, raising the possibility that members of this rare cohort may not
324 be bona-fide LARP7 family members, at least as these are currently appreciated [20]. Based on
325 the observed distribution, it seems likely that both genes were present in a fungi common
326 ancestor, but Pof8 or both Bin3 and Pof8 were lost in certain lineages. Examination of the
327 distribution of Bin3 and LARP7-family members in basal eukaryotic lineages reveals a similar
328 pattern: Bin3 can be present without LARP7, but there are no instances where a LARP7-family
329 member exists in a lineage lacking a Bin3 homolog (Table S8). Similarly, LARP7-family proteins
330 are represented in Alveolates, Stramenopiles, Amoebozoa, Fungi, and Metazoans, while Bin3-

331 family proteins are present in all eukaryotic lineages. Since the presence of Pof8/LARP7 is very
332 highly linked to the presence of a Bin3 homolog, these data suggest that the function of LARP7
333 family members may be more intimately associated with the function of Bin3/MePCE than has
334 been previously appreciated.
335
336 **Discussion:**
337 In this study, we have identified Bin3 as a novel component of the *S. pombe* telomerase
338 holoenzyme. In addition to showing an interaction between Bin3 and U6 snRNA, we
339 demonstrate that Bin3 interacts with the telomerase RNA TER1 and components of the active
340 telomerase holoenzyme in a manner that is dependent on the presence of the LARP7 family
341 protein Pof8. Together, our results indicating that Bin3 interacts with the mature, spliced form
342 of TER1 and that Bin3 immunoprecipitates possess telomerase activity *in vitro* strongly suggest
343 that Bin3 is a constitutive component of the telomerase holoenzyme containing Trt1, Pof8,
344 Lsm2-8, and Est1 scaffolded on TER1 (Figure 4E). Our results are in agreement with recent
345 findings from the Baumann lab reporting the presence of Bin3/Bmc1 in the telomerase
346 holoenzyme [50]. The idea of Pof8 and Bin3 scaffolded on TER1 is reminiscent of LARP7 and
347 MePCE in the 7SK snRNP, with Pof8/LARP7 recruiting Bin3/MePCE to the RNA substrate. Similar
348 to our data showing Pof8 recruiting Bin3 to TER1 and the telomerase holoenzyme, LARP7 has
349 also been demonstrated to recruit MePCE to the 7SK snRNP in human cells [24]. Thus, the
350 protein-protein interaction and subsequent recruitment to RNA substrates by LARP7 appears
351 evolutionarily conserved in fission yeast and higher eukaryotes. We also present data
352 demonstrating that the presence of Pof8-like proteins is nearly universally correlated with the

353 presence of Bin3-like proteins in fungi, suggesting that the Bin3-Pof8 interaction is highly
354 conserved and more prevalent than previously anticipated. Since Pof8 is required to load Bin3
355 onto the telomerase RNA and U6 snRNA in fission yeast, this phylogenetic distribution raises
356 the question of whether Bin3 homologs in fungi lacking a LARP7 homolog have evolved a
357 mechanism to bind RNA targets in a Pof8/LARP7 independent fashion.
358
359 Since TER1 undergoes several processing steps before assembly into the telomerase
360 holoenzyme, we were able to assess TER1 processing state to determine when Bin3 interacts
361 with TER1 with respect to the timing of TER1 maturation. We show that Bin3-associated TER1
362 has a mature 3' end, indicative of spliceosome-catalyzed end processing, and a 5' TMG cap. This
363 is consistent with previously reported data on the timing of Pof8 binding; since our data
364 indicates that the interaction between Bin3 and TER1 is dependent on Pof8, the most
365 parsimonious explanation is that Pof8, and thus Bin3, bind TER1 following 3' maturation and
366 TMG capping, preceding the binding of the Lsm2-8 complex [13]. We show that the interaction
367 between Bin3 and TER1 is dependent on Pof8, leading to the conclusion that Bin3 interacts with
368 TER1 at the same stage as Pof8, resulting in the hierarchical assembly of the active telomerase
369 holoenzyme.
370
371 The finding that Bin3-associated TER1 is immunoprecipitated by a TMG antibody argues against
372 a catalytic role for Bin3 in TER1 processing. Our data, coupled with previous work characterizing
373 the cap structure on the mature TER1 bound to Trt1 [3,4], supports the idea that Bin3 has a
374 capping-independent function in the telomerase holoenzyme. LARP7 binding to MePCE in the

375 7SK snRNP inhibits its capping activity; MePCE, in turn, promotes the interaction between 7SK
376 and LARP7, thereby stabilizing the complex [34]. In the *S. pombe* telomerase holoenzyme and U6
377 snRNP, we can hypothesize that Pof8 may also inhibit the methyltransferase activity of Bin3 by
378 binding to and occluding the active site. This is consistent with our results suggesting a transient
379 interaction between Pof8 and U6 that may function to load Bin3 on U6. In such a model, an
380 interaction between Bin3 and Pof8 is necessary to recruit Bin3 to U6 and following dissociation
381 of Pof8, the catalytic site of Bin3 would become available to cap U6. It is curious to note that
382 Bin3 deletion has no effect on U6 levels (Figure 5B), although such a finding is consistent with
383 what has been observed for human U6 upon MePCE depletion [26]. Since the lack of an MePCE-
384 catalyzed cap on human 7SK is associated with an increase in exonucleolytic degradation[26], this
385 therefore raises the question as to the function of the γ-monomethyl phosphate cap on U6, if
386 not to protect the 5' end from exonucleolytic degradation.
387
388 Additionally, our work identifying Bin3 as a telomerase-associated protein brings to mind work
389 identifying a box H/ACA motif at the 3' end of vertebrate telomerase RNA [51]. Box H/ACA RNAs
390 form an RNP complex with Dyskerin/Cbf5, Nop10, Nhp2, and Gar1 to guide noncoding RNA
391 pseudouridylation [52,53]. Although Dyskerin is a pseudouridine synthase, to date no evidence has
392 pointed to a modification function for Dyskerin in the context of telomerase RNA. Rather, the
393 Dyskerin-containing H/ACA complex has a structural role in telomerase biogenesis, with binding
394 of the H/ACA RNP to telomerase RNA leading to a conformational change in the RNA that
395 promotes 3' processing and maturation over exosome-mediated decay [54]. This is reminiscent of
396 the apparent catalytic independent role we observed for Bin3 in fission yeast telomerase,

397 although our data point towards Bin3 having a role promoting Pof8 binding to TER1, perhaps
398 also through Bin3-mediated conformational changes in TER1. The decreased TER1 levels
399 observed upon Bin3 deletion (Figure 5A) can likely be attributed to the decreased interaction
400 between Pof8 and TER1 in the absence of Bin3. We therefore propose a model in which the
401 direct interaction between Bin3 and Pof8 both recruits Bin3 to the telomerase holoenzyme, as
402 well as promotes Pof8 binding to TER1. This in turn promotes Lsm2-8 binding to the exposed 3'
403 end of TER1, which protects TER1 from exosome-mediated degradation [13,15,16]. The resulting
404 TER1-containing RNP then recruits Trt1, forming a stable complex capable of extending
405 telomeres.
406
407 Another facet of this work builds on the idea that components of the telomerase holoenzyme
408 are more conserved than previously appreciated. In addition to the ubiquitous telomerase
409 reverse transcriptase, previous work has identified LARP7 family proteins in both ciliates and
410 yeast [11,13–15], arguing a level of evolutionary conservation. We now also provide evidence
411 indicating the presence of RNase P and RNase MRP subunits in fission yeast, much like the
412 RNase P and RNase MRP subunits found in the budding yeast telomerase complex [38–40]. The
413 presence of RNase P and RNase MRP subunits in two divergent yeast species supports the
414 importance of these factors in the function of a breadth of telomerase holoenzymes.
415
416 Our results indicating that Bin3 is part of the telomerase holoenzyme were quite unexpected,
417 as Bin3 has been well-characterized in higher eukaryotes for its role in the processing,
418 maturation, and protection of RNA Polymerase III transcripts [26,34]. An intriguing idea involves

419 polymerase switching through telomerase RNA evolution. Ciliate telomerase RNA is transcribed
420 by RNA Polymerase III and subsequently binds the LARP7 homolog p65 through the terminal
421 polyuridylate stretch common to RNA Polymerase III transcripts [11,17]. Since MePCE and LARP7
422 also associate with RNA Polymerase III transcripts, it is possible that the Pof8-bound RNA
423 Polymerase II transcribed TER1, and the *S. pombe* telomerase RNP as a whole, represent an
424 intermediate step in the evolution of telomerase RNA between ciliates and the RNA Polymerase
425 II transcribed telomerase RNA of higher eukaryotes. Future work should investigate the
426 presence of Bin3/MePCE homologs in the telomerase holoenzymes of other species,
427 particularly in ciliates, which possess both an RNA Polymerase III transcribed telomerase RNA
428 and a LARP7 homolog. Such findings will continue to develop emerging ideas regarding
429 conservation in telomerase RNA processing and the composition of telomerase RNPs.
430

431 **Acknowledgements:**
432 We thank Toru Nakamura and Virginia Zakian for sharing published yeast strains and Marc
433 Fabian and Raymund Wellinger for helpful comments on the manuscript. J.P. is supported by a
434 Canada Graduate Scholarship (Doctoral) from the National Sciences and Engineering Research
435 Council of Canada. M.A.B. is supported by a Discovery Grant from NSERC ("Impact of chemical
436 modification of non-coding RNAs on gene expression in *S. pombe*"). JMD is supported by the
437 Institut Universitaire de France (IUF), JMD and MEB by the CNRS and the University of
438 Perpignan (UPVD) and their study is set within the framework of the "Laboratoires
439 d'Excellences (LABEX)" TULIP (ANR-10-LABX-41) and of the "École Universitaire de Recherche
440 (EUR)" TULIP-GS (ANR-18-EURE-0019).

441

442 **Author contributions:**

443 J.P. conceived of the study, designed, performed, and analyzed all experiments, and wrote the
444 first draft of the manuscript with input from all authors. M.E.B. and J-M.D. performed
445 phylogenetic analyses. J.P. analyzed RNA-Seq data with help from J.G.. M.A.B. conceived of the
446 study, designed experiments, supervised the project, and edited the manuscript.

447

448 **Materials and Methods:**

449 Strains, constructs, and growth media

450 Strains were grown in yeast extract with supplements (YES) or Edinburgh Minimal Media
451 (EMM), as indicated. Tag integration and knockouts were generated with a previously described
452 PCR-based strategy and verified by PCR and western blotting [55] (primer sequences in Table S5).
453 Protein A-tagged strains were generated according to [56]. The Bin3 knockout strain was
454 constructed by replacing the Bin3 open reading frame with the phleomycin resistance cassette
455 and flanking primers containing 750 nucleotides of homology to the Bin3 genomic locus.
456 Correct genotypes were selected on YES plates with the corresponding antibiotic (200 μg/mL
457 G418, Sigma; 100 μg/mL Nourseothricin, GoldBio; 100 μg/mL phleomycin, Invivogen). Other
458 strains were created by mating and antibiotic selection. A list of strains is provided in Table S4.

459

460 Native protein extract and immunoprecipitation

461 *S. pombe* cells were grown in YES at 32°C to mid-log phase, harvested, and subject to cryogenic
462 disruption using a mortar and pestle. Cell powder was lysed in 50 mM NaCl, 20 mM Hepes pH

463 7.4, 55 mM KOAc, 0.5% Triton X, 0.1% Tween-20, 0.2 mM PMSF, 1:100 Protease Inhibitor
464 Cocktail (Thermo, 78430), and 0.004 U/μL RNase inhibitor (Invitrogen, AM2694). For Protein A-
465 tagged strains, immunoprecipitation was carried out with Rabbit IgG-conjugated (MP-
466 Biomedicals, SKU 085594) Dynabeads (Invitrogen, 14301) as described [57]. Myc-tagged proteins
467 were immunoprecipitated with Protein G Dynabeads (Invitrogen, 10003D) coated with anti-myc
468 antibody (Cell Signaling, 2276S). Beads were washed 4 times with 400 μL lysis buffer. For RNA
469 immunoprecipitations, bound RNA was isolated by treatment of beads with 0.1% SDS and 0.2
470 mg/mL Proteinase K (Sigma, P2308) at 37°C for 30 minutes, followed by extraction with phenol:
471 chloroform:isoamyl alcohol (25:24:1) and ethanol precipitation.
472
473 RNA preparation and Northern blotting
474 Total RNA was isolated from 1% of native protein extracts by incubation with 0.5% SDS, 0.2
475 mg/mL proteinase K (Sigma, P2308), 20 mM Tris HCl pH 7.4, and 10 mM EDTA pH 8.0 for 15
476 minutes at 50°C, followed by phenol: chloroform extraction and ethanol precipitation. Northern
477 blot analysis was performed as described using 8% TBE-urea polyacrylamide gels [58]. Briefly,
478 electrophoresed RNA was transferred to positively charged nylon membranes (Perkin Elmer,
479 NEF988001) with the iBlot 2 system (Thermo, IB21001) and probed with ^{32}P γ-ATP-labeled DNA
480 probes (probe sequences provided in Table S6). For RNase H digestion, RNA was incubated with
481 25 pmol RNase H probe (provided in Table S6) for 5 minutes at 65°C and slow cooled to 37°C,
482 followed by digestion with 5 U RNase H (NEB, M02975) for 30 minutes at 37°C. The reaction
483 was stopped with the addition of 25 μM EDTA pH 8.0 and phenol: chloroform extraction and
484 ethanol precipitation. TMG-capped RNAs were isolated from RNase H-treated

485 immunoprecipitates with Protein G Dynabeads coated with an α-TMG antibody (Sigma,

486 MABE302), according to [59].

487

488 qRT-PCR and semi-quantitative RT-PCR

489 1 μg Turbo DNase-treated RNA was reverse transcribed with the iScript cDNA synthesis kit

490 (BioRad, 1708890), treated with 0.5 μL RNase cocktail (Invitrogen, AM2286), and diluted 1:10.

491 cDNA was quantified using the SensiFAST SYBR No-Rox kit (Bioline, BIO-98005) and 1 μM of

492 each primer (primer sequences provided in Table S6). qPCR settings were as follows: 95°C for

493 10 minutes and 40 cycles consisting of 10 seconds at 95°C, 20 seconds at 60°C, and 20 seconds

494 at 72°C, followed by melting curve analysis. TER1 and U6 levels were normalized to act1 mRNA

495 levels and subsequently subject to paired two-tailed student's *t*-tests and, where applicable,

496 one-way ANOVA followed by a Tukey posthoc test with α set to 0.05 (Table S10).

497

498 For semi-quantitative RT-PCR, DNase-treated RNA, 10 nmol dNTP mix, and 10 pmol gene-

499 specific reverse primers (Table S6) were heated to 65°C and slow-cooled to 37°C before reverse

500 transcription with 5 U AMV-RT (NEB, M0277L) at 42°C for 1 hour. cDNA was amplified with Taq

501 Polymerase (NEB, MO273L) using standard protocols and the following cycling conditions: 5

502 minute initial denaturation at 94°C, 22 (TER1) or 17 (U6) cycles of 30 seconds at 94°C, 30

503 seconds at 57°C, and 1 minute at 72°C, and a final 10 minute extension at 72°C.

504

505 RIP Seq

506 Libraries were constructed from immunoprecipitated RNA samples by the RNomics Platform at
507 the Université de Sherbrooke in Sherbrooke, Quebec. RNA quality was assessed with a
508 Bioanalyzer small RNA chip (Agilent, 5067-1548). Libraries were constructed with the NEBNext
509 Ultra II Directional Kit (NEB, E7760S) and amplified with 10 PCR cycles. cDNA libraries were
510 sequenced on an Illumina NextSeq 500 with 2 runs per sample, each for 50-bp single-end reads.
511 Following fastp processing (Version 0.20.1), reads from the first sequencing run were aligned to
512 the fission yeast genome (ASM294v2) with Bowtie 2 [60,61] and counted with featurecounts [62]
513 using the EF2 build of the ENSEMBL fission yeast genome. Differential expression analysis was
514 performed using edgeR, with reads filtered to include transcripts with at least 1 CPM in each
515 sample and libraries were normalized by TMM[63,64].
516
517 Circularized Rapid Amplification of cDNA Ends (cRACE)
518 Immunoprecipitated RNA was treated with 2 U TURBO DNase (Invitrogen, AM2239) and
519 dephosphorylated with 1 U calf intestinal alkaline phosphatase (NEB, M0290), followed by
520 decapping and circularization with RNA 5' Pyrophosphohydrolase (NEB, M0356S) and T4 RNA
521 Ligase 1 (NEB, M0204S). TER1 was amplified from circularized RNA with the OneStep RT-PCR Kit
522 (Qiagen, 210210) (primer sequences in Table S6). cRACE products were cloned into the pGEM-T
523 vector (Promega, A1360) and sequenced by the TCAG DNA Sequencing Facility at the Hospital
524 for Sick Children in Toronto.
525
526 Mass spectrometry and GO analysis

527 Half of the native protein extract was pre-treated with 0.625 U/μL Benzonase (Millipore, E1014)
528 at 37°C for 30 minutes. The reaction was stopped with 5 mM EDTA pH 8.0 and Protein A
529 immunoprecipitation was performed in the same manner as for RNA immunoprecipitations.
530 After washes with lysis buffer, beads were washed with 0.1 M NH_4OAc and 0.1 mM $MgCl_2$ and
531 eluted with 0.5 M NH_4OH for 20 minutes at room temperature. Eluates were lyophilized and
532 subject to in-solution tryptic digestion. LC-MS/MS analysis was performed by the IRCM
533 Proteomics Discovery Platform on a Q Exactive HF.
534
535 Raw data was processed and analyzed using the MaxQuant software package 1.5.1.2 [65] and the
536 fission yeast UP000002485 reference proteome (24/11/2019). Settings used for MaxQuant
537 analysis were as reported [66]. Proteins present in immunoprecipitations from both biological
538 replicates and absent from control immunoprecipitations were considered genuine Bin3
539 interacting partners and ranked by peak intensity. PANTHER overrepresentation tests (GO
540 Ontology database released 2019-12-09) were conducted on the top 50 Bin3 interacting
541 partners. Fisher's exact tests with FDR correction were performed using the GO biological
542 process complete and GO cellular component complete data sets.
543
544 Co-immunoprecipitation and western blotting
545 *S. pombe* cells were grown in YES at 32°C to mid-log phase, harvested, and subject to cryogenic
546 disruption using a mortar and pestle. Cell power was lysed in Co-IP lysis buffer (10 mM Tris HCl
547 pH 7.5, 150 mM NaCl, 0.5% NP40, 1:100 Protease Inhibitor Cocktail). Immunoprecipitations
548 were carried out as described and proteins were eluted by resuspending beads in 2X SDS

549 loading buffer (100 mM Tris HCl pH 6.8, 4% SDS, 20% glycerol, 0.2% bromophenol blue) and
550 boiling at 95°C for 5 minutes. Western blot analyses were performed using monoclonal anti-
551 myc (Cell Signaling, 2276S) at 1:5000 and monoclonal anti-beta actin (abcam, ab8226) at 1:2500
552 for primary antibodies and HRP-conjugated anti-mouse at 1:5000 for secondary antibodies.
553 Protein A-tagged proteins were detected with HRP-conjugated polyclonal anti-Protein A
554 (Invitrogen, PA1-26853) at 1:5000.
555
556 Glycerol gradient sedimentation
557 Native protein extracts were separated on a 10 mL 20-50% glycerol gradient (20 mM HEPES pH
558 7.6, 1 mM MgOAc, 1 mM DTT, 300 mM KOAc) and spun in an SW41 rotor for 20 hours at 30,000
559 rpm according to [67]. Individual fractions were divided in 2 for protein extraction by TCA
560 precipitation and RNA extraction with phenol: chloroform.
561
562 Telomerase activity assay
563 The telomerase activity assay was performed as described [13]. Briefly, bead slurries (see
564 immunoprecipitation) were incubated at 30°C for 90 minutes in a 10 μL reaction containing 50
565 mM Tris HCl pH 8.0, 1 mM MgOAc, 5% glycerol, 1 mM spermidine, 1 mM DTT, 100 mM KOAc,
566 0.2 mM dATP, dCTP, and dTTP, 5 μM telomerase assay primer (Table S6), and 0.3 μM 3000
567 Ci/mmol [α-^{32}P] dGTP (Perkin Elmer, BLU512H250UC). The reaction was stopped with the
568 addition of 0.5% SDS, 10 mM EDTA pH 8.0, 20 mM Tris HCl pH 7.5, 2 μg/μL Proteinase K
569 (Sigma), and 1000 cpm [γ-^{32}P] ATP-labeled 100-mer oligonucleotide and incubation at 42°C for
570 15 minutes, followed by phenol: chloroform extraction and ethanol precipitation. RNase A-

571 treated samples were pre-incubated with 20 ng RNase A (Invitrogen, AM2271) at 30°C for 10
572 minutes. Extension products were separated on a 10% urea-TBE polyacrylamide sequencing gel
573 at 60 W for 90 minutes, dried and exposed to a PhosphorScreen, and imaged with a Typhoon
574 imager.
575
576 Genomic DNA extraction, southern blotting, and chromosome fusion PCR
577 Genomic DNA was extracted from logarithmically growing cells according to [14]. For southern
578 blotting, 15 μg genomic DNA was digested overnight with EcoRI or ApaI and separated on a 1%
579 agarose gel, transferred to positively charged nylon membranes (Perkin Elmer, NEF988001) by
580 capillary transfer in 10X SSC, and probed with a ^{32}P γ-ATP-labeled telomere probe (probe
581 sequence provided in Table S6). The chromosome fusion PCR was adapted from [13]. Briefly, 50
582 μL PCR reactions contained 1 μL genomic DNA, 0.4 μM forward and reverse primers (sequences
583 provided in Table S6), 200 μM dNTPs, 1X Taq ThermoPol Buffer (NEB), and 1.25 U Taq
584 Polymerase (NEB, M0273). The Trt1 gene was amplified as a loading control in an identical PCR
585 reaction containing the corresponding primers. The PCR reaction consisted of an initial
586 denaturation at 95°C for 5 minutes, followed by 32 cycles of 95°C for 15 seconds, 55°C for 30
587 seconds, and 68°C for 3 minutes, with a final extension at 68°C for 10 minutes.
588
589 Structure prediction
590 The structure of *S. pombe* Bin3 was predicted using Phyre2 [68] and aligned with the co-crystal
591 structure of the *H. sapiens* MePCE methyltransferase domain bound to 7SK snRNA and SAH

592 (6DCB [31]) in PyMol [69]. Primary sequences were aligned with the Clustal Omega Multiple
593 Sequence Alignment tool [70].
594
595 Phylogenetic tree construction and search for Bin3-like and Pof8-like sequences
596 Protein sequences (GeneCatalogs) of 472 fungal species were downloaded from the JGI website
597 (https://mycocosm.jgi.doe.gov/) in fasta format. 5614520 proteins were downloaded and
598 merged into a single multifasta file. A blast (Blastp) against all proteins was performed using
599 diamond blastp [71] with a minimum e-value of 1e-5 and outfmt 6 (for tabular output). In order to
600 identify homologous proteins, proteins were clustered together if they shared at least 50%
601 similarity over 70% of coverage using SiLiX [72]. When a cluster contained two or more paralogous
602 genes derived from duplications, the species was removed from the cluster. Finally, only
603 clusters with a minimum of 100 species were retained for further analysis. Following these
604 cleaning steps, we obtained 5328 clusters containing one gene per species. Proteins sequences
605 of each cluster were aligned using MAFFT (v7.271) with default parameters
606 (https://mafft.cbrc.jp/alignment/server/). Multiple alignments were cleaned using trimA1
607 (v1.4.rev22 build [2015-05-21]) with -st 0.01 option. Fastree (version 2.1.10 SSE3) with default
608 parameters were used to build phylogenetic trees [73]. The consensus fungi tree was obtained
609 using ASTRAL (astral.5.6.3) software with default parameters [74]. To detect the presence of
610 genes coding for Bin3-like and Pof8-like proteins, blast searches (blastp and tbalstn) were
611 performed on each studied fungus genome, using initially either the full-length *S. pombe* Bin3
612 protein sequence or the *S. pombe* Pof8 xRRM conserved motif. This procedure was repeated in
613 each fungal clade using clade-specific Bin3-like and Pof8-like sequences detected by the initial

614 search using *S. pombe* sequences. Finally, new blast searches were performed all over again,
615 this time using Bin3-like or Pof8-like "probes" made of a collection of sequences representing
616 the diversity of these two proteins in fungi.
617
618 Data availability
619 The mass spectrometry proteomics data have been deposited to the ProteomeXchange
620 Consortium via the PRIDE [75] partner repository with the dataset identifier PDX023356 and
621 10.6019/PDX023356 (reviewer account details: username: reviewer_pxd023356@ebi.ac.ul
622 password: M2zPpwXx). RNA Seq data have been deposited in NCBI's Sequence Read Archive
623 (SRA) database under BioProject number PRJNA776661
624 (reviewer link:
625 https://dataview.ncbi.nlm.nih.gov/object/PRJNA776661?reviewer=af5gv098pam3mdt9rsb2rtsl
626 ci).
627
628 **References:**

629 1. Blackburn, E. H. & Collins, K. Telomerase: An RNP enzyme synthesizes DNA. *Cold Spring*
630 *Harb. Perspect. Biol.* (2011) doi:10.1101/cshperspect.a003558.
631 2. Collins, K. The biogenesis and regulation of telomerase holoenzymes. *Nature Reviews*
632 *Molecular Cell Biology* (2006) doi:10.1038/nrm1961.
633 3. Leonardi, J., Box, J. A., Bunch, J. T. & Baumann, P. TER1, the RNA subunit of fission yeast
634 telomerase. *Nat. Struct. Mol. Biol.* (2008) doi:10.1038/nsmb1343.
635 4. Webb, C. J. & Zakian, V. A. Identification and characterization of the

636 Schizosaccharomyces pombe TER1 telomerase RNA. *Nat. Struct. Mol. Biol.* (2008)
637 doi:10.1038/nsmb1354.
638 5. Nakamura, T. M. *et al.* Telomerase catalytic subunit homologs from fission yeast and
639 human. *Science (80-.).* (1997) doi:10.1126/science.277.5328.955.
640 6. Greider, C. W. & Blackburn, E. H. A telomeric sequence in the RNA of Tetrahymena
641 telomerase required for telomere repeat synthesis. *Nature* (1989)
642 doi:10.1038/337331a0.
643 7. Chapon, C., Cech, T. R. & Zaug, A. J. Polyadenylation of telomerase RNA in budding yeast.
644 *RNA* (1997).
645 8. Feng, J. *et al.* The RNA component of human telomerase. *Science (80-.).* (1995)
646 doi:10.1126/science.7544491.
647 9. Box, J. A., Bunch, J. T., Tang, W. & Baumann, P. Spliceosomal cleavage generates the 3'
648 end of telomerase RNA. *Nature* (2008) doi:10.1038/nature07584.
649 10. Tang, W., Kannan, R., Blanchette, M. & Baumann, P. Telomerase RNA biogenesis involves
650 sequential binding by Sm and Lsm complexes. *Nature* (2012) doi:10.1038/nature10924.
651 11. Witkin, K. L. & Collins, K. Holoenzyme proteins required for the physiological assembly
652 and activity of telomerase. *Genes Dev.* (2004) doi:10.1101/gad.1201704.
653 12. O'Connor, C. M. & Collins, K. A Novel RNA Binding Domain in Tetrahymena Telomerase
654 p65 Initiates Hierarchical Assembly of Telomerase Holoenzyme. *Mol. Cell. Biol.* (2006)
655 doi:10.1128/mcb.26.6.2029-2036.2006.
656 13. Páez-Moscoso, D. J. *et al.* Pof8 is a La-related protein and a constitutive component of
657 telomerase in fission yeast. *Nat. Commun.* (2018) doi:10.1038/s41467-017-02284-8.

658 14. Mennie, A. K., Moser, B. A. & Nakamura, T. M. LARP7-like protein Pof8 regulates
659 telomerase assembly and poly(A)+TERRA expression in fission yeast. *Nat. Commun.*
660 (2018) doi:10.1038/s41467-018-02874-0.
661 15. Collopy, L. C. *et al.* LARP7 family proteins have conserved function in telomerase
662 assembly. *Nat. Commun.* (2018) doi:10.1038/s41467-017-02296-4.
663 16. Hu, X. *et al.* Quality-Control Mechanism for Telomerase RNA Folding in the Cell. *Cell Rep.*
664 (2020) doi:10.1016/j.celrep.2020.108568.
665 17. Singh, M. *et al.* Structural Basis for Telomerase RNA Recognition and RNP Assembly by
666 the Holoenzyme La Family Protein p65. *Mol. Cell* (2012)
667 doi:10.1016/j.molcel.2012.05.018.
668 18. Singh, M., Choi, C. P. & Feigon, J. xRRM: A new class of RRM found in the telomerase La
669 family protein p65. *RNA Biol.* (2013) doi:10.4161/rna.23608.
670 19. Basu, R., Eichhorn, C. D., Cheng, R., Peterson, R. D. & Feigon, J. Structure of S. pombe
671 telomerase protein Pof8 C-terminal domain is an xRRM conserved among LARP7
672 proteins. *RNA Biol.* (2020) doi:10.1080/15476286.2020.1836891.
673 20. Deragon, J.-M. M. Distribution, organization an evolutionary history of La and LARPs in
674 eukaryotes. *RNA Biol.* 1–9 (2020) doi:10.1080/15476286.2020.1739930.
675 21. Nguyen, V. T., Kiss, T., Michels, A. A. & Bensaude, O. 7SK small nuclear RNA binds to and
676 inhibits the activity of CDK9/cyclin T complexes. *Nature* (2001) doi:10.1038/35104581.
677 22. Yang, Z., Zhu, Q., Luo, K. & Zhou, Q. The 7SK small nuclear RNA inhibits the CDK9/cyclin
678 T1 kinase to control transcription. *Nature* (2001) doi:10.1038/35104575.
679 23. Krueger, B. J. *et al.* LARP7 is a stable component of the 7SK snRNP while P-TEFb, HEXIM1

680 and hnRNP A1 are reversibly associated. *Nucleic Acids Res.* (2008)
681 doi:10.1093/nar/gkn061.
682 24. Muniz, L., Egloff, S. & Kiss, T. RNA elements directing in vivo assembly of the
683 7SK/MePCE/Larp7 transcriptional regulatory snRNP. *Nucleic Acids Res.* (2013)
684 doi:10.1093/nar/gkt159.
685 25. Eichhorn, C. D., Chug, R. & Feigon, J. hLARP7 C-terminal domain contains an xRRM that
686 binds the 3' hairpin of 7SK RNA. *Nucleic Acids Res.* (2016) doi:10.1093/nar/gkw833.
687 26. Jeronimo, C. *et al.* Systematic Analysis of the Protein Interaction Network for the Human
688 Transcription Machinery Reveals the Identity of the 7SK Capping Enzyme. *Mol. Cell*
689 (2007) doi:10.1016/j.molcel.2007.06.027.
690 27. Cosgrove, M. S., Ding, Y., Rennie, W. A., Lane, M. J. & Hanes, S. D. The bin3 RNA
691 methyltransferase targets 7SK RNA to control transcription and translation. *Wiley*
692 *Interdisciplinary Reviews: RNA* (2012) doi:10.1080/09540121.2017.1344767.
693 28. Xhemalce, B., Robson, S. C. & Kouzarides, T. Human RNA methyltransferase BCDIN3D
694 regulates MicroRNA processing. *Cell* (2012) doi:10.1016/j.cell.2012.08.041.
695 29. Martinez, A. *et al.* Human BCDIN3D monomethylates cytoplasmic histidine transfer RNA.
696 *Nucleic Acids Res.* (2017) doi:10.1093/nar/gkx051.
697 30. Marz, M. *et al.* Evolution of 7SK RNA and its protein partners in metazoa. *Mol. Biol. Evol.*
698 (2009) doi:10.1093/molbev/msp198.
699 31. Yang, Y., Eichhorn, C. D., Wang, Y., Cascio, D. & Feigon, J. Structural basis of 7SK RNA 5'-γ-
700 phosphate methylation and retention by MePCE. *Nat. Chem. Biol.* (2019)
701 doi:10.1038/s41589-018-0188-z.

702 32. Tani, T. & Ohshima, Y. The gene for the U6 small nuclear RNA in fission yeast has an
703 intron. *Nature* (1989) doi:10.1038/337087a0.
704 33. Tani, T. & Ohshima, Y. mRNA-type introns in U6 small nuclear RNA genes: Implications for
705 the catalysis in pre-mRNA splicing. *Genes Dev.* (1991) doi:10.1101/gad.5.6.1022.
706 34. Xue, Y., Yang, Z., Chen, R. & Zhou, Q. A capping-independent function of MePCE in
707 stabilizing 7SK snRNA and facilitating the assembly of 7SK snRNP. *Nucleic Acids Res.*
708 (2009) doi:10.1093/nar/gkp977.
709 35. Gu, J., Patton, J. R., Shimba, S. & Reddy, R. Localization of modified nucleotides in
710 Schizosaccharomyces pombe spliceosomal small nuclear RNAs: Modified nucleotides are
711 clustered in functionally important regions. *RNA* (1996).
712 36. Beernink, H. T. H., Miller, K., Deshpande, A., Bucher, P. & Cooper, J. P. Telomere
713 maintenance in fission yeast requires an est1 ortholog. *Curr. Biol.* (2003)
714 doi:10.1016/S0960-9822(03)00169-6.
715 37. Webb, C. J. & Zakian, V. A. Schizosaccharomyces pombe Ccq1 and TER1 bind the 14-3-3-
716 like domain of Est1, which promotes and stabilizes telomerase-telomere association.
717 *Genes Dev.* (2012) doi:10.1101/gad.181826.111.
718 38. Lemieux, B. *et al.* Active Yeast Telomerase Shares Subunits with Ribonucleoproteins
719 RNase P and RNase MRP. *Cell* (2016) doi:10.1016/j.cell.2016.04.018.
720 39. Garcia, P. D. *et al.* Stability and nuclear localization of yeast telomerase depend on
721 protein components of RNase P/MRP. *Nat. Commun.* (2020) doi:10.1038/s41467-020-
722 15875-9.
723 40. Laterreur, N. *et al.* The yeast telomerase module for telomere recruitment requires a

724 specific RNA architecture. *RNA* **24**, (2018).

725 41. Zappulla, D. C. & Cech, T. R. Yeast telomerase RNA: A flexible scaffold for protein
726 subunits. *Proc. Natl. Acad. Sci. U. S. A.* (2004) doi:10.1073/pnas.0403641101.

727 42. Barboric, M. *et al.* 7SK snRNP/P-TEFb couples transcription elongation with alternative
728 splicing and is essential for vertebrate development. *Proc. Natl. Acad. Sci. U. S. A.* (2009)
729 doi:10.1073/pnas.0903188106.

730 43. Hasler, D. *et al.* The Alazami Syndrome-Associated Protein LARP7 Guides U6 Small
731 Nuclear RNA Modification and Contributes to Splicing Robustness. *Mol. Cell* (2020)
732 doi:10.1016/j.molcel.2020.01.001.

733 44. Wang, X. *et al.* LARP7-Mediated U6 snRNA Modification Ensures Splicing Fidelity and
734 Spermatogenesis in Mice. *Mol. Cell* (2020) doi:10.1016/j.molcel.2020.01.002.

735 45. Hayles, J. *et al.* A genome-wide resource of cell cycle and cell shape genes of fission
736 yeast. *Open Biol.* (2013) doi:10.1098/rsob.130053.

737 46. Kim, D. U. *et al.* Analysis of a genome-wide set of gene deletions in the fission yeast
738 Schizosaccharomyces pombe. *Nat. Biotechnol.* (2010) doi:10.1038/nbt.1628.

739 47. Lee, N. N. *et al.* XMtr4-like protein coordinates nuclear RNA processing for
740 heterochromatin assembly and for telomere maintenance. *Cell* **155**, (2013).

741 48. Coy, S., Volanakis, A., Shah, S. & Vasiljeva, L. The Sm Complex Is Required for the
742 Processing of Non-Coding RNAs by the Exosome. *PLoS One* **8**, (2013).

743 49. Nakamura, T. M., Cooper, J. P. & Cech, T. R. Two modes of survival of fission yeast
744 without telomerase. *Science* vol. 282 (1998).

745 50. Paez-Moscoso, D. J. *et al.* A putative cap binding protein and the methyl phosphate

746 capping enzyme Bin3/MePCE function in telomerase biogenesis. *bioRxiv*
747 2021.12.15.472819 (2021) doi:10.1101/2021.12.15.472819.
748 51. Mitchell, J. R., Cheng, J. & Collins, K. A Box H/ACA Small Nucleolar RNA-Like Domain at
749 the Human Telomerase RNA 3' End. *Mol. Cell. Biol.* (1999) doi:10.1128/mcb.19.1.567.
750 52. Matera, A. G., Terns, R. M. & Terns, M. P. Non-coding RNAs: Lessons from the small
751 nuclear and small nucleolar RNAs. *Nature Reviews Molecular Cell Biology* (2007)
752 doi:10.1038/nrm2124.
753 53. Lafontaine, D. L. J., Bousquet-Antonelli, C., Henry, Y., Caizergues-Ferrer, M. & Tollervey,
754 D. The box H + ACA snoRNAs carry Cbf5p, the putative rRNA pseudouridine synthase.
755 *Genes Dev.* (1998) doi:10.1101/gad.12.4.527.
756 54. Tseng, C. K., Wang, H. F., Schroeder, M. R. & Baumann, P. The H/ACA complex disrupts
757 triplex in hTR precursor to permit processing by RRP6 and PARN. *Nat. Commun.* (2018)
758 doi:10.1038/s41467-018-07822-6.
759 55. Bähler, J. *et al.* Heterologous modules for efficient and versatile PCR-based gene
760 targeting in Schizosaccharomyces pombe. *Yeast* (1998) doi:10.1002/(SICI)1097-
761 0061(199807)14:10<943::AID-YEA292>3.0.CO;2-Y.
762 56. Oeffinger, M. *et al.* Comprehensive analysis of diverse ribonucleoprotein complexes. *Nat.*
763 *Methods* (2007) doi:10.1038/nmeth1101.
764 57. Vakiloroayaei, A., Shah, N. S., Oeffinger, M. & Bayfield, M. A. The RNA chaperone La
765 promotes pre-tRNA maturation via indiscriminate binding of both native and misfolded
766 targets. *Nucleic Acids Res.* **45**, 11341–11355 (2017).
767 58. Porat, J. & Bayfield, M. A. Use of tRNA-Mediated Suppression to Assess RNA Chaperone

768 Function. in *RNA Chaperones: Methods and Protocols* (ed. Heise, T.) 107–120 (Springer
769 US, 2020). doi:10.1007/978-1-0716-0231-7_6.
770 59. Hayes, K. E., Barr, J. A., Xie, M., Steitz, J. A. & Martinez, I. Immunoprecipitation of Tri-
771 methylated Capped RNA. *Bio-protocol* **8**, e2717 (2018).
772 60. Langmead, B. & Salzberg, S. L. Fast gapped-read alignment with Bowtie 2. *Nat. Methods*
773 **9**, (2012).
774 61. Langmead, B., Trapnell, C., Pop, M. & Salzberg, S. L. Ultrafast and memory-efficient
775 alignment of short DNA sequences to the human genome. *Genome Biol.* **10**, (2009).
776 62. Liao, Y., Smyth, G. K. & Shi, W. FeatureCounts: An efficient general purpose program for
777 assigning sequence reads to genomic features. *Bioinformatics* **30**, (2014).
778 63. Liu, R. *et al.* Why weight? Modelling sample and observational level variability improves
779 power in RNA-seq analyses. *Nucleic Acids Res.* **43**, (2015).
780 64. Robinson, M. D., McCarthy, D. J. & Smyth, G. K. edgeR: A Bioconductor package for
781 differential expression analysis of digital gene expression data. *Bioinformatics* **26**, (2009).
782 65. Cox, J. & Mann, M. MaxQuant enables high peptide identification rates, individualized
783 p.p.b.-range mass accuracies and proteome-wide protein quantification. *Nat. Biotechnol.*
784 (2008) doi:10.1038/nbt.1511.
785 66. Drissi, R., Dubois, M. L., Douziech, M. & Boisvert, F. M. Quantitative proteomics reveals
786 dynamic interactions of the minichromosome maintenance complex (MCM) in the
787 cellular response to etoposide induced DNA damage. *Mol. Cell. Proteomics* (2015)
788 doi:10.1074/mcp.M115.048991.
789 67. Lue, N. F. & Peng, Y. Identification and characterization of a telomerase activity from

790 Schizosaccharomyces pombe. *Nucleic Acids Res.* **25**, 4331–4337 (1997).

791 68. Kelley, L. A., Mezulis, S., Yates, C. M., Wass, M. N. & Sternberg, M. J. E. The Phyre2 web
792 portal for protein modeling, prediction and analysis. *Nat. Protoc.* (2015)
793 doi:10.1038/nprot.2015.053.

794 69. DeLano, W. L. The PyMOL Molecular Graphics System, Version 1.8. *Schrödinger LLC*
795 (2014) doi:10.1038/hr.2014.17.

796 70. Sievers, F. & Higgins, D. G. Clustal Omega. *Curr. Protoc. Bioinforma.* (2014)
797 doi:10.1002/0471250953.bi0313s48.

798 71. Buchfink, B., Xie, C. & Huson, D. H. Fast and sensitive protein alignment using DIAMOND.
799 *Nature Methods* (2014) doi:10.1038/nmeth.3176.

800 72. Miele, V., Penel, S. & Duret, L. Ultra-fast sequence clustering from similarity networks
801 with SiLiX. *BMC Bioinformatics* (2011) doi:10.1186/1471-2105-12-116.

802 73. Price, M. N., Dehal, P. S. & Arkin, A. P. FastTree 2 - Approximately maximum-likelihood
803 trees for large alignments. *PLoS One* (2010) doi:10.1371/journal.pone.0009490.

804 74. Mirarab, S. *et al.* ASTRAL: Genome-scale coalescent-based species tree estimation. in
805 *Bioinformatics* (2014). doi:10.1093/bioinformatics/btu462.

806 75. Perez-Riverol, Y. *et al.* The PRIDE database and related tools and resources in 2019:
807 Improving support for quantification data. *Nucleic Acids Res.* (2019)
808 doi:10.1093/nar/gky1106.

809

810 **Figure Legends:**

811

812 **Figure 1: Bin3 interacts with U6 snRNA and the telomerase RNA TER1**

813 A) Enrichment of Bin3 PrA immunoprecipitated transcripts compared to an untagged control

814 (biological replicates = 3). Axes represent log2 of fold change and negative log of false discovery

815 rate.

816 B) Northern blot analysis of the mature and intron-containing U6 from total RNA and PrA

817 immunoprecipitates from untagged (wild type, wt) and PrA-tagged Bin3 strains.

818 C) Northern blot of the telomerase RNA TER1, U6, and U5 from total RNA and PrA

819 immunoprecipitates from untagged and PrA-tagged Bin3 strains, and semi-quantitative RT-PCR

820 analysis of TER1.

821

822 **Figure 2: Bin3 interacts with the same TER1 species as well-established components of the**

823 **telomerase holoenzyme**

824 A) The 5' and 3' ends of Bin3-, Trt1-, Pof8-, and Lsm3-associated TER1 were identified by cRACE.

825 The results of 10 independent clones per immunoprecipitation are shown below a schematic of

826 the architecture of TER1.

827 B) RNase H northern blots of RNase H-generated 5' and 3' ends of TER1 immunoprecipitated by

828 various telomerase components. The same blot was stripped and reprobed for U6.

829 C-D) Northern blot of α-TMG flow through (FT) and immunoprecipitated (IP) transcripts from

830 total RNA (C) and Bin3-associated RNA (D).

831

832 **Figure 3: Bin3 interacts with components of the mature telomerase holoenzyme**

833 A) Gene ontology analysis (biological process) of top 50 Bin3 protein interactors.

834 B-C) Examination and nucleic acid-dependence of interactions between Bin3 and Pof8 (B) and
835 Bin3 and Trt1 (C) by co-immunoprecipitation and western blotting. Blots were reprobed for
836 beta actin as a loading control.
837
838 **Figure 4: Bin3 is recruited to the active telomerase holoenzyme by Pof8**
839 A) Northern blot and semi-quantitative RT-PCR of TER1 and U6 in PrA immunoprecipitates for
840 an untagged wild type (wt), PrA-tagged (Bin3 PrA), and PrA-tagged Pof8 knockout strain (Bin3
841 PrA ΔPof8). Bin3-PrA was detected in input and immunoprecipitated samples by western blots
842 probing for PrA (bottom panel). Possible cleavage products are indicated with an asterisk.
843 B) qRT-PCR of TER1 and U6 in Bin3 PrA immunoprecipitates from a wild type and *pof8Δ* strain
844 normalized to input RNA. Relative TER1 and U6 IP was calculated by comparing percent
845 immunoprecipitation of TER1 or U6 to immunoprecipitation from an untagged strain (mean ±
846 standard error, paired *t* test * at $p < 0.05$, ** at $p < 0.01$, *** at $p < 0.001$, and **** at $p<0.0001$)
847 (n=2 biological replicates).
848 C) Northern blot of mature and intron-containing U6 in PrA- and myc-tagged
849 immunoprecipitated RNA.
850 D) Telomerase assay of PrA-tagged Bin3 in a wild type and *pof8Δ* strain. A ^{32}P-labeled 100-mer
851 oligonucleotide was used as a loading control. Telomerase extension products were compared
852 to a terminal transferase ladder, with +1 and +4 extension products indicated. Western blot
853 probing for PrA following PrA immunoprecipitation is shown in the panel below.

854 E) Proposed model of the fission yeast telomerase holoenzyme. TER1 structure and binding
855 locations are based on models constructed by Hu and colleagues[16] and Mennie and
856 colleagues[14].
857
858 **Figure 5: Bin3 promotes TER1 accumulation and Pof8 recruitment to telomerase**
859 A) Quantitation of TER1 and U6 in total RNA by qRT-PCR, normalized to act1 mRNA. P-values
860 over bars represent comparison to a wild type strain (mean ± standard error, paired *t* test *
861 at $p < 0.05$, ** at $p < 0.01$, *** at $p < 0.001$, and **** at $p<0.0001$) (n=3 biological replicates).
862 B) Southern blot comparing telomere length in following 3 restreaks on rich media (one
863 restreak= 20-25 generations). Genomic DNA was digested with EcoRI (left) or ApaI (right) to
864 yield different sized telomere restriction fragments.
865 C) qRT-PCR of TER1 in Pof8 myc immunoprecipitates from a wild type and *bin3Δ* strain
866 normalized to input RNA. Relative TER1 IP was calculated by comparing percent
867 immunoprecipitation of TER1 to immunoprecipitation from an untagged strain (mean ±
868 standard error, paired *t* test * at $p < 0.05$, ** at $p < 0.01$, *** at $p < 0.001$, and **** at $p<0.0001$)
869 (n=2 biological replicates). P-values over each bar represent results of a paired t-test with Pof8
870 myc.
871 D) Telomerase assay of myc-tagged Pof8 in a wild type and *bin3Δ* strain. A ^{32}P-labeled 100-mer
872 oligonucleotide was used as a loading control. Telomerase extension products were compared
873 to a terminal transferase ladder, with +1 and +4 extension products indicated. Western blot
874 probing for myc following myc immunoprecipitation is shown in the panel below.

875 E-F) Relative telomerase extension activity for myc-tagged Pof8 immunoprecipitates in a wild
876 type and *bin3Δ* strain. The intensity of the +4 extension product was normalized to a
877 precipitation loading control, then further normalized to TER1 expression (E) or the amount of
878 TER1 immunoprecipitated with Pof8 (F). P-values over each bar represent results of a paired t-
879 test with Pof8 myc (n=4).
880
881 **Figure 6: Phylogenic distribution of Bin3 and Pof8 in fungi**
882 Consensus cladogram describing the phylogenic relationships of 472 species representative of
883 fungi phylum and classes and highlighting (using a color code) the distribution of Bin3 and Pof8
884 in these species. The cladogram is a consensus tree of 5328 distinct protein coding gene trees
885 resulting from a genome-wide, against all, protein comparison (see Materials and Methods).
886 Only posterior probabilities inferior to 1 are shown. The Bin3 and Pof8 distribution is
887 recapitulated in Supplemental Table 8 with corresponding protein sequences. A cartoon
888 presenting structural domains of Pof8 is presented. Pof8 La module and RRM1 are only inferred
889 from secondary structure predictions and are represented by *La** and *RRM1** in the
890 corresponding cartoon. In four species (colored in orange in the cladogram) only an N-terminal
891 truncated version of Pof8 (Pof8*) that cannot accommodate the La module is present. Full
892 cladogram with species names and statistical supports of the different nodes is presented in
893 Figure S7.
894
895 **Supplementary figure captions:**
896

897 **Supplementary figure 1: Bin3 is the *S. pombe* methyl phosphate capping enzyme (MePCE)**

898 **homolog**

899 A) Schematic of the domain architecture of Bin3 homologs from *S. pombe*, *H. sapiens,* and *D.*

900 *melanogaster*.

901 B) Clustal alignment of the methyltransferase/SAM-binding domains of *S. pombe* Bin3, *H.*

902 *sapiens* MePCE, and *D. melanogaster* Bin3. Predicted SAM-binding residues are indicated in red

903 and nucleotide-binding residues are in blue.

904 C) Phyre2[68] structure prediction of *S. pombe* Bin3 bound to a 5' terminal guanosine (orange)

905 and SAH (green). Predicted SAM-binding residues are in red and nucleotide-binding residues

906 are in blue.

907

908 **Supplementary figure 2: Reciprocal co-immunoprecipitations validate an interaction between**

909 **Bin3 and Pof8**

910 The interaction between Bin3 and Pof8 was confirmed by α-myc co-immunoprecipitation.

911

912 **Supplementary figure 3: Glycerol gradient sedimentation of Bin3, Pof8, TER1, and U6 in a wild**

913 **type and *pof8Δ* strain**

914 Western blot and semi-quantitative RT-PCR of Bin3 PrA, Pof8 myc, TER1, and U6 in gradient

915 fractions.

916

917 **Supplementary figure 4: Bin3 overexpression fails to rescue *pof8Δ*-dependent telomere**

918 **defects**

919 A) Chromosome fusion PCR (top) following 2 restreaks on minimal media (one re-streak= 20-25
920 generations) from wild type and *pof8Δ* strains overexpressing an empty vector (pRep4x) or
921 Bin3. The Trt1 gene was amplified from genomic DNA as a loading control (bottom).
922 B) Southern blot comparing telomere length from the same genomic DNA as (A). Genomic DNA
923 was digested with EcoRI.
924
925 **Supplementary figure 5: Validation of a Bin3 knockout strain confirms its viability**
926 A) Schematic of Bin3 knockout (top) and PCR validation of the resultant strain using the
927 indicated primers.
928 B) qRT-PCR of bin3 mRNA normalized to act1 mRNA for wild type and *bin3Δ* strains (mean ±
929 standard error, paired *t* test * at $p < 0.05$, ** at $p < 0.01$, *** at $p < 0.001$, and **** at $p<0.0001$)
930 (n=3 biological replicates). P-values over each bar represent results of a paired t-test with a wild
931 type strain.
932 C) Backcrossing of *bin3Δ* and a wild type strain, followed by tetrad dissection, confirms viability
933 of the *bin3Δ* strain on rich media. Tetrads from the same spore are arranged in columns.
934 Resulting haploid colonies possessing phleomycin resistance are circled in red and colonies that
935 didn't grow after tetrad dissection are circled in black.
936 D) qRT-PCR of TER1 normalized to act1 mRNA for wild type and *bin3Δ* strains transformed with
937 an empty vector (3x) or Bin3 (mean ± standard error, paired *t* test * at $p < 0.05$, ** at $p < 0.01$,
938 *** at $p < 0.001$, and **** at $p<0.0001$) (n=3 biological replicates). P-values over each bar
939 represent results of a paired t-test with a wild type strain transformed with an empty vector
940 (wild type + pRep3x).

941

942 **Supplementary figure 6: Bin3 and Pof8 are not strictly required for telomere maintenance**

943 Southern blot comparing ApaI-digested genomic DNA isolated after 5 restreaks on rich media. A

944 lack of signal with a telomeric probe represents survivors that have lost telomeric DNA and

945 circularized their chromosomes (*TER1Δ*).

946

947 **Supplementary figure 7: Phylogenic distribution of Bin3 and Pof8 in fungi**

948 Complete consensus cladogram describing the phylogenic relationships of 472 species

949 representative of fungi phylum and classes and highlighting (using a color code) the distribution

950 of Bin3 and Pof8 in these species. Only posterior probabilities inferior to 1 are shown.

951

952

922 Resulting haploid colonies possessing phleomycin resistance are circled in red and colonies that
923 didn't grow after tetrad dissection are circled in black.
924 D) qRT-PCR of TER1 normalized to act1 mRNA for wild type and *bin3Δ* strains transformed with
925 an empty vector (3x) or Bin3 (mean ± standard error, paired *t* test * at $p > 0.05$, ** at $p < 0.01$,
926 *** at $p < 0.001$, and **** at $p<0.0001$) (n=3 biological replicates). P-values over each bar
927 represent results of a paired t-test with a wild type strain transformed with an empty vector
928 (wild type + pRep3x).
929
930 **Supplementary figure 6: Bin3 and Pof8 are not strictly required for telomere maintenance**
931 Southern blot comparing ApaI-digested genomic DNA isolated after 5 restreaks on rich media. A
932 lack of signal with a telomeric probe represents survivors that have lost telomeric DNA and
933 circularized their chromosomes (*TER1Δ*).
934
935 **Supplementary figure 7: Phylogenic distribution of Bin3 and Pof8 in fungi**
936 Complete consensus cladogram describing the phylogenic relationships of 472 species
937 representative of fungi phylum and classes and highlighting (using a color code) the distribution
938 of Bin3 and Pof8 in these species. Only posterior probabilities inferior to 1 are shown.
939
940

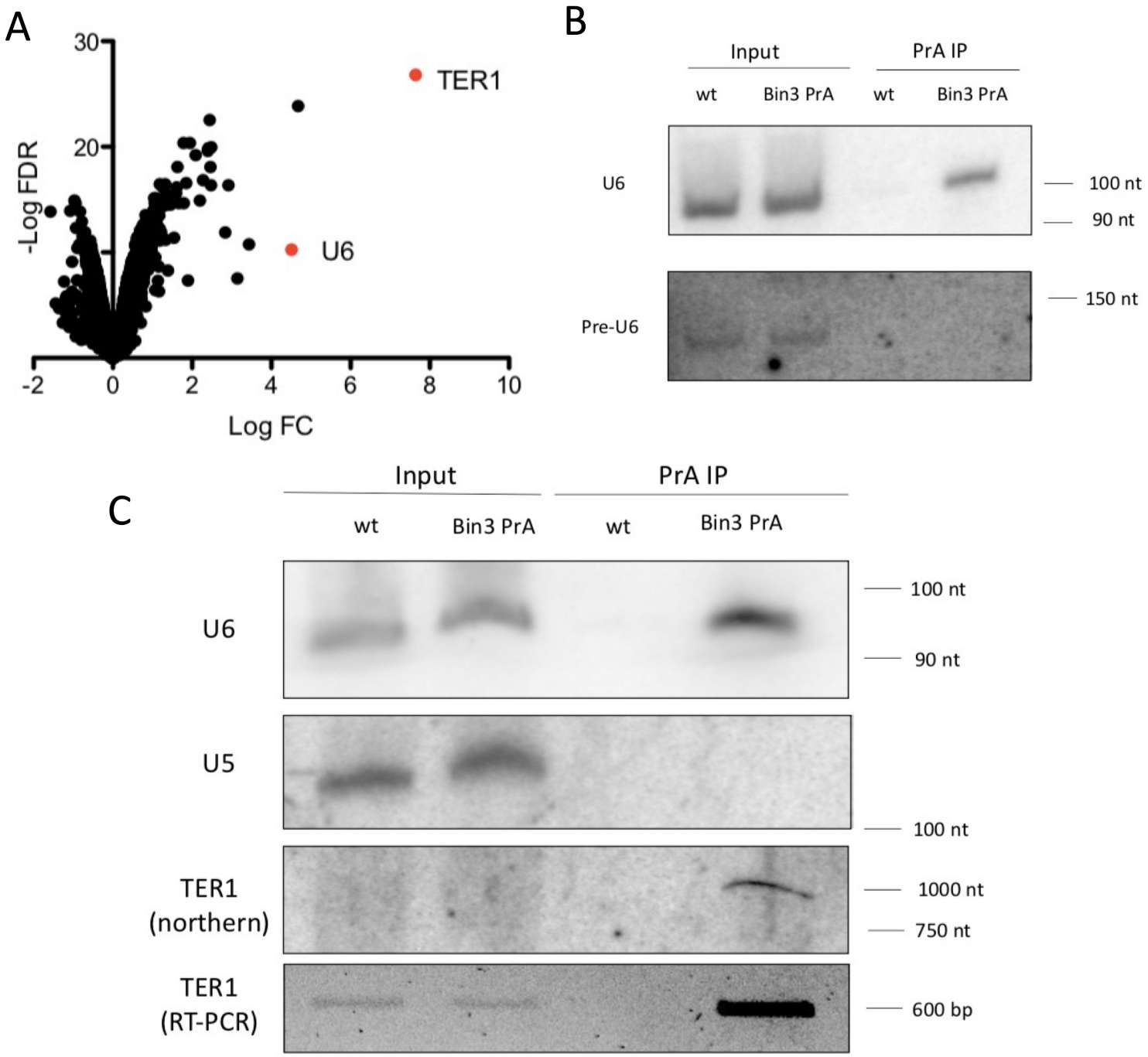

Figure 1: Bin3 interacts with U6 snRNA and the telomerase RNA TER1

A) Enrichment of Bin3 PrA immunoprecipitated transcripts compared to an untagged control (biological replicates = 3). Axes represent log2 of fold change and negative log of false discovery rate.

B) Northern blot analysis of the mature and intron-containing U6 from total RNA and PrA immunoprecipitates from untagged (wild type, wt) and PrA-tagged Bin3 strains.

C) Northern blot of the telomerase RNA TER1, U6, and U5 from total RNA and PrA immunoprecipitates from untagged and PrA-tagged Bin3 strains, and semi-quantitative RT-PCR analysis of TER1.

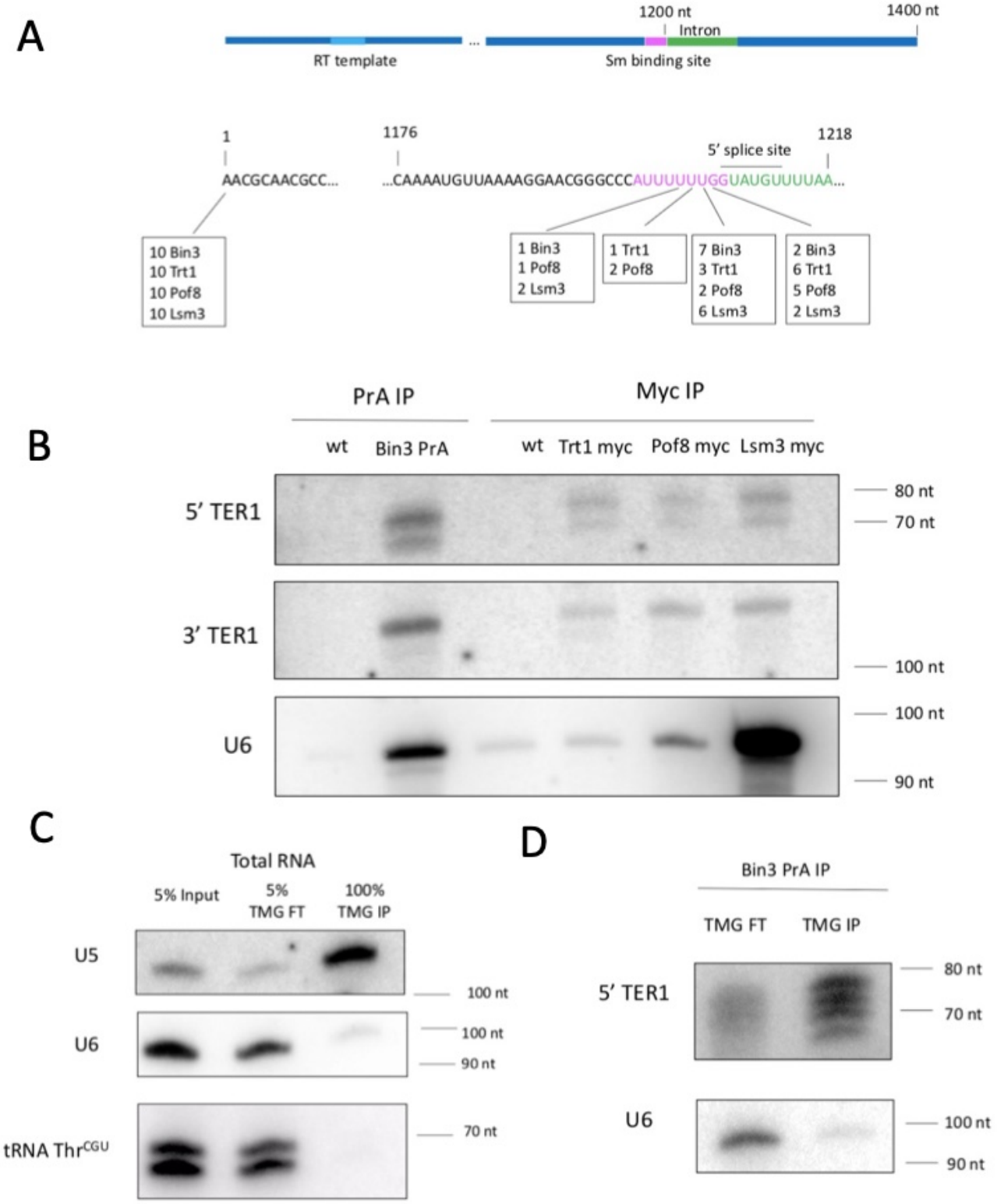

Figure 2: Bin3 interacts with the same TER1 species as well-established components of the telomerase holoenzyme

A) The 5' and 3' ends of Bin3-, Trt1-, Pof8-, and Lsm3-associated TER1 were identified by cRACE. The results of 10 independent clones per immunoprecipitation are shown below a schematic of the architecture of TER1.

B) RNase H northern blots of RNase H-generated 5' and 3' ends of TER1 immunoprecipitated by various telomerase components. The same blot was stripped and reprobed for U6.

C-D) Northern blot of a-TMG flow through (FT) and immunoprecipitated (IP) transcripts from total RNA (C) and Bin3-associated RNA (D).

A

GO biological process	Fold enrichment	Raw P value	False discovery rate
Telomerase holoenzyme complex assembly	49.39	2.04E-08	5.33E-05
Telomere maintenance via telomerase	31.75	2.54E-04	4.74E-02
RNA-dependent DNA biosynthetic process	31.75	2.54E-04	4.58E-02
Ribonucleoprotein complex assembly	5.47	6.70E-06	2.50E-03
Ribonucleoprotein complex subunit organization	5.29	9.01E-06	2.77E-03
mRNA cis splicing, via spliceosome	5.25	6.76E-05	1.54E-02
mRNA splicing, via spliceosome	4.78	5.48E-05	1.43E-02
RNA splicing, via transesterification reactions with bulged adenosine as nucleophile	4.78	5.48E-05	1.43E-02
RNA splicing, via transesterification reactions	4.72	6.08E-05	1.45E-02
RNA splicing	4.52	8.60E-05	1.80E-02

B

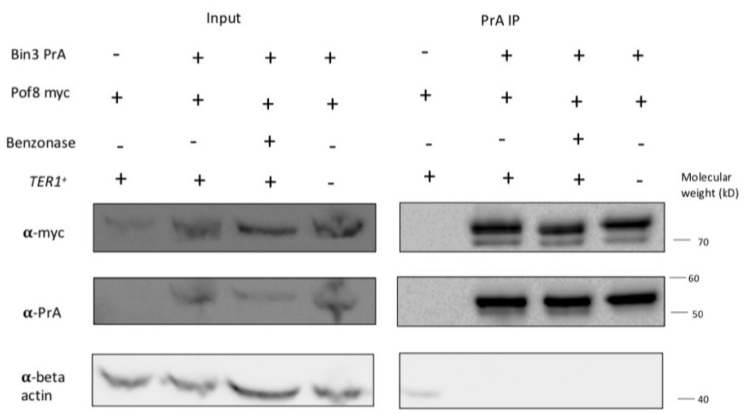

C

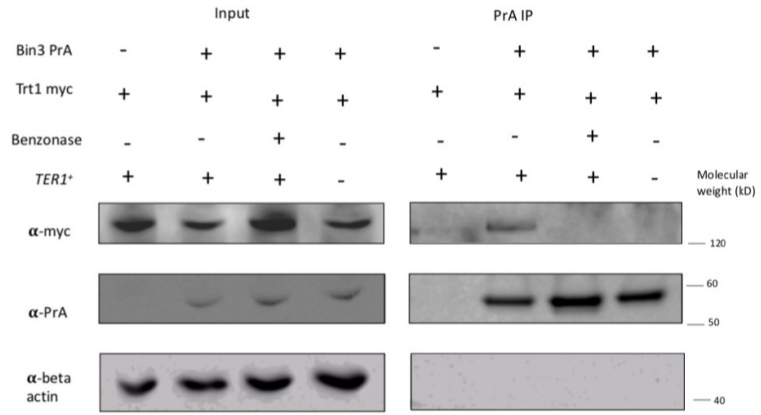

Figure 3: Bin3 interacts with components of the mature telomerase holoenzyme

A) Gene ontology analysis (biological process) of top 50 Bin3 protein interactors.

B-C) Examination and nucleic acid-dependence of interactions between Bin3 and Pof8 (B) and Bin3 and Trt1 (C) by co-immunoprecipitation and western blotting. Blots were reprobed for beta actin as a loading control.

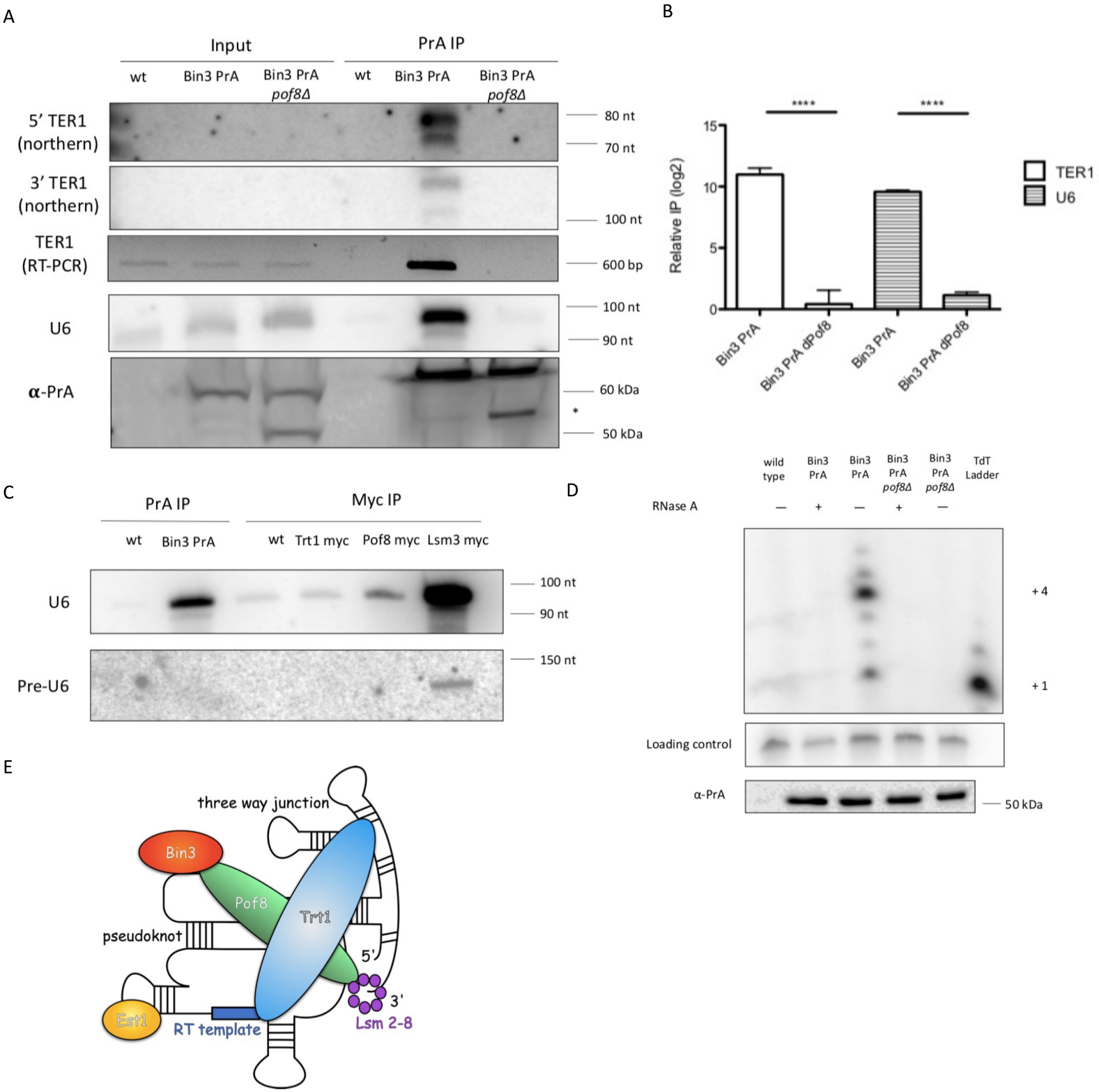

Figure 4: Bin3 is recruited to the active telomerase holoenzyme by Pof8

A) Northern blot and semi-quantitative RT-PCR of TER1 and U6 in PrA immunoprecipitates for an untagged wild type (wt), PrA-tagged (Bin3 PrA), and PrA-tagged Pof8 knockout strain (Bin3 PrA ΔPof8). Bin3-PrA was detected in input and immunoprecipitated samples by western blots probing for PrA (bottom panel). Possible cleavage products are indicated with an asterisk.

B) qRT-PCR of TER1 and U6 in Bin3 PrA immunoprecipitates from a wild type and pof8Δ strain normalized to input RNA. Relative TER1 and U6 IP was calculated by comparing percent immunoprecipitation of TER1 or U6 to immunoprecipitation from an untagged strain (mean ± standard error, paired t test * at $p < 0.05$, ** at $p < 0.01$, *** at $p < 0.001$, and **** at $p<0.0001$) (n=2 biological replicates).

C) Northern blot of mature and intron-containing U6 in PrA- and myc-tagged immunoprecipitated RNA.

D) Telomerase assay of PrA-tagged Bin3 in a wild type and pof8Δ strain. A 32P-labeled 100-mer oligonucleotide was used as a loading control. Telomerase extension products were compared to a terminal transferase ladder, with +1 and +4 extension products indicated. Western blot probing for PrA following PrA immunoprecipitation is shown in the panel below.

E) Proposed model of the fission yeast telomerase holoenzyme. TER1 structure and binding locations are based on models constructed by Hu and colleagues16 and Mennie and colleagues14.

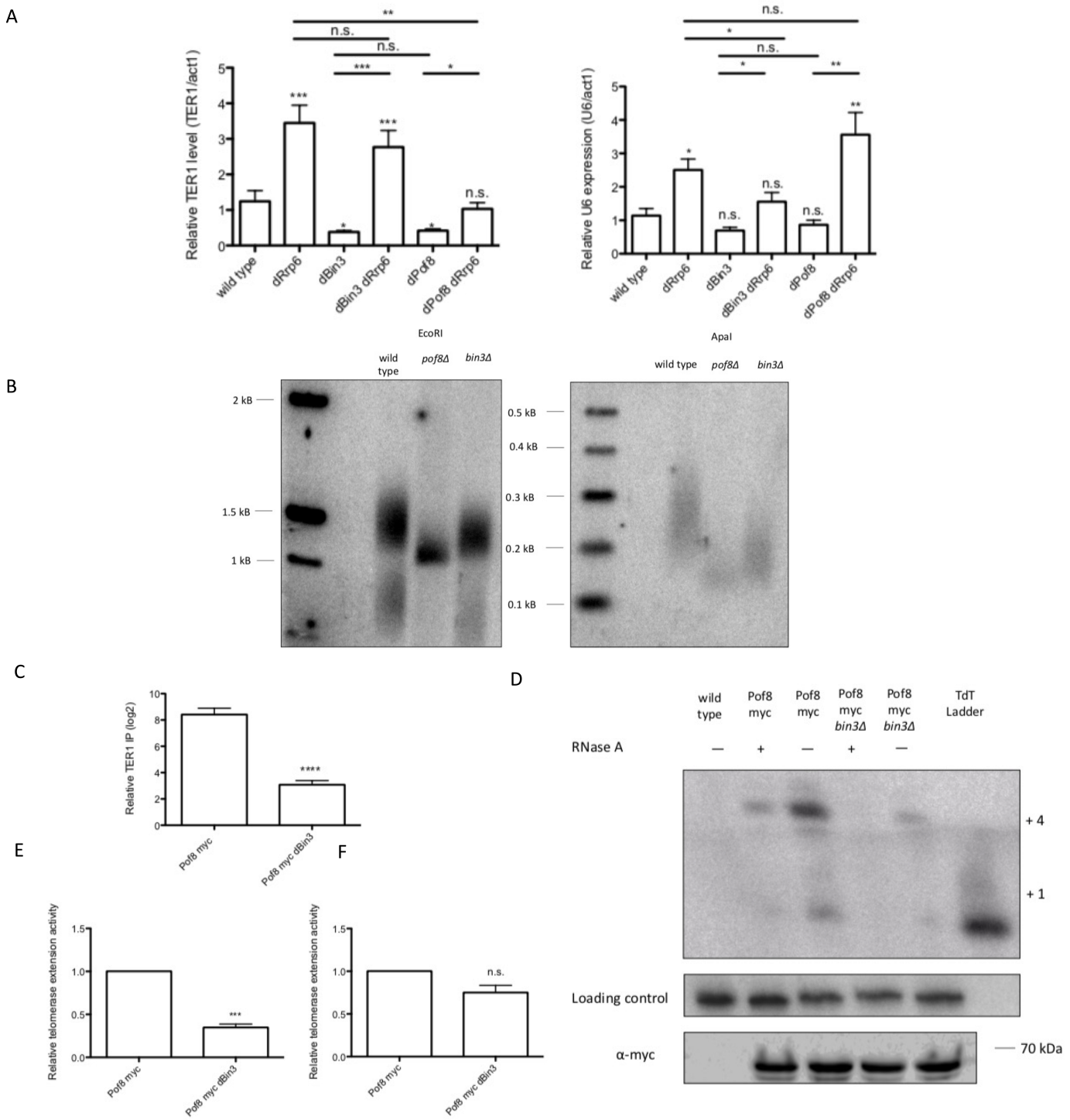

Figure 5: Bin3 promotes TER1 accumulation and Pof8 recruitment to telomerase

A) Quantitation of TER1 and U6 in total RNA by qRT-PCR, normalized to act1 mRNA. P-values over bars represent comparison to a wild type strain (mean ± standard error, paired t test * at $p < 0.05$, ** at $p < 0.01$, *** at $p < 0.001$, and **** at $p<0.0001$) (n=3 biological replicates).
B) Southern blot comparing telomere length in following 3 restreaks on rich media (one restreak= 20-25 generations). Genomic DNA was digested with EcoRI (left) or ApaI (right) to yield different sized telomere restriction fragments.
C) qRT-PCR of TER1 in Pof8 myc immunoprecipitates from a wild type and bin3Δ strain normalized to input RNA. Relative TER1 IP was calculated by comparing percent immunoprecipitation of TER1 to immunoprecipitation from an untagged strain (mean ± standard error, paired t test * at $p < 0.05$, ** at $p < 0.01$, *** at $p < 0.001$, and **** at $p<0.0001$) (n=2 biological replicates). P-values over each bar represent results of a paired t-test with Pof8 myc.
D) Telomerase assay of myc-tagged Pof8 in a wild type and bin3Δ strain. A 32P-labeled 100-mer oligonucleotide was used as a loading control. Telomerase extension products were compared to a terminal transferase ladder, with +1 and +4 extension products indicated. Western blot probing for myc following myc immunoprecipitation is shown in the panel below.
E-F) Relative telomerase extension activity for myc-tagged Pof8 immunoprecipitates in a wild type and bin3Δ strain. The intensity of the +4 extension product was normalized to a precipitation loading control, then further normalized to TER1 expression (E) or the amount of TER1 immunoprecipitated with Pof8 (F). P-values over each bar represent results of a paired t-test with Pof8 myc (n=4).

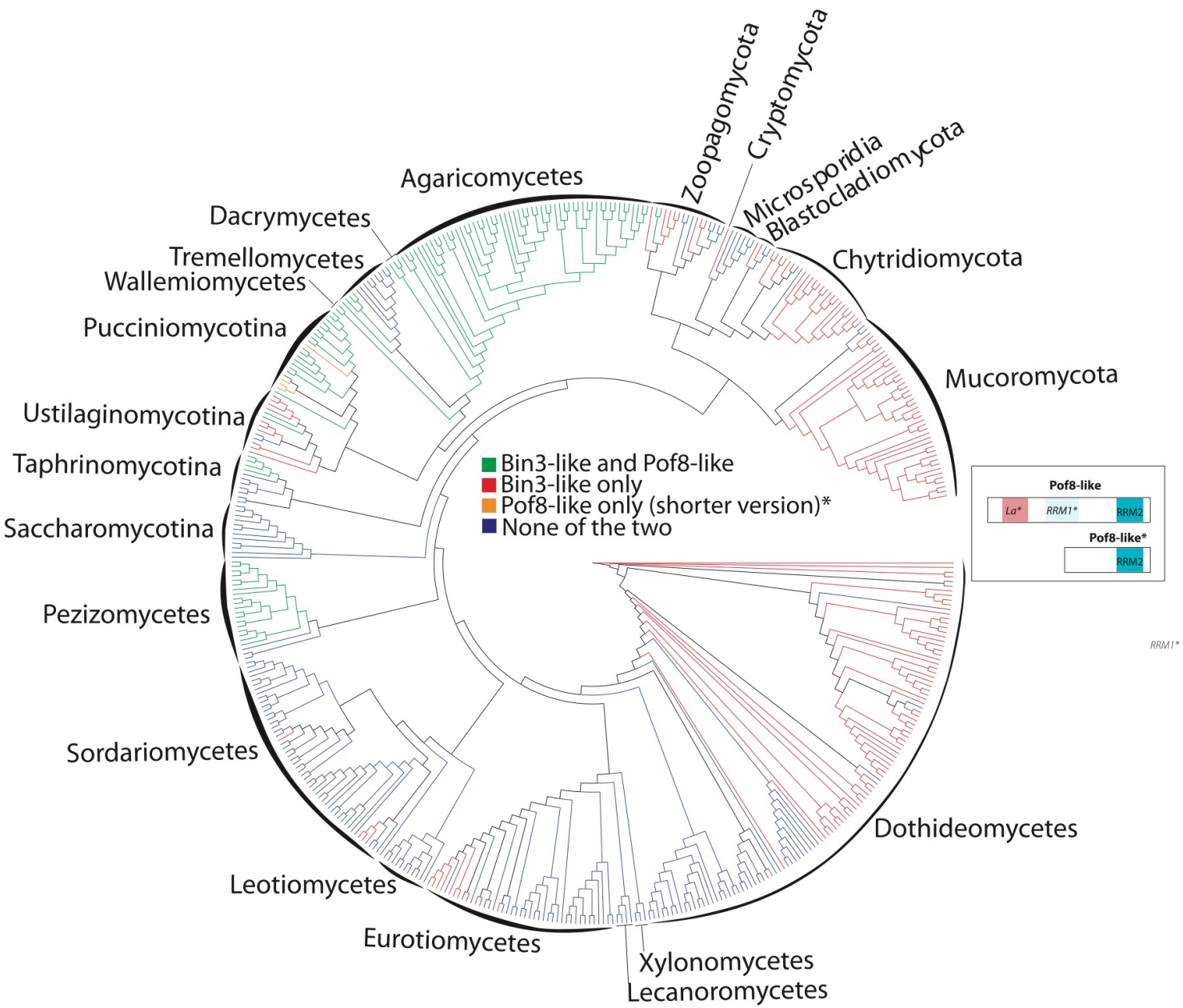

Figure 6: Phylogenic distribution of Bin3 and Pof8 in fungi

Consensus cladogram describing the phylogenic relationships of 472 species representative of fungi phylum and classes and highlighting (using a color code) the distribution of Bin3 and Pof8 in these species. The cladogram is a consensus tree of 5328 distinct protein coding gene trees resulting from a genome-wide, against all, protein comparison (see Materials and Methods). Only posterior probabilities inferior to 1 are shown. The Bin3 and Pof8 distribution is recapitulated in Supplemental Table 8 with corresponding protein sequences. A cartoon presenting structural domains of Pof8 is presented. Pof8 La module and RRM1 are only inferred from secondary structure predictions and are represented by *La** and *RRM1** in the corresponding cartoon. In four species (colored in orange in the cladogram) only an N-terminal truncated version of Pof8 (Pof8*) that cannot accommodate the La module is present. Full cladogram with species names and statistical supports of the different nodes is presented in Figure S7.

A

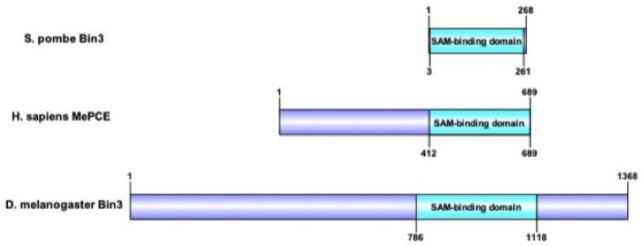

B

```
S.pombe          MSNFQHGNYHSYYSMRGGTSIIDPRLKCL--PDSLFYEASVLDIGCNNGTVSAQIASIFG    58
H.sapiens        --KFQYGNYCKYYGYRNPSC-EDGRLRVL--KPEWFRGRDVLDLGCNVGHLTLSIACKWG    55
D.melanogaster   --KYRYGNFDRYVDFRQMNEFRDVRLQVFQRHVELFENKDILDIGCNVGHMTITVARHLA    58
                   ::::**:  * . *  .   * **: :    . *   .:**:*** * ::  :*   .

S.pombe          ASFVLGLDIDHVLIQKARKHLEFVSSRIG---PV--------------------------    89
H.sapiens        PSRMVGLDIDSRLIHSARQNIRHYLSEELRLPPQTLEGDPGAEGEE--------------    101
D.melanogaster   PKTIVGIDIDRELVARARRNLSIFVRIPKEEKLLEVKAEPTVDAKANIAVKDETSGAAHK    118
                  . ::*:***  *:  **:::

S.pombe          -------------------------------RNPGSIVEDQFNYYPISSIKKFSRIPVQL    118
H.sapiens        ----------------------------------GTTTVRKRSCFPASLTASRGPI----    123
D.melanogaster   KTRRGKRRRKVHQGIHHHHHHHHHDLEQLQQQQKLNSLLVKPHEFFPISFPLTYGRIPRIL    178
                                                  .:      . :* *   . . *

S.pombe          QPP------LNKQNFPHNIEFETADFLR------WESKRKFKIILAISVSKWVHLNNHDE    166
H.sapiens        AAPQVPLDGADTSVFPNNVVFVTGNYVLDRDDLVEAQTPEYDVVLCLSLTKWVHLNWGDE    183
D.melanogaster   SSSKSPNMLGNKNQFPANVFFRHTNYVLKDESLMASDTQQYDLILCLSVTKWIHLNFGDN    238
                            :.. ** *: *   :::          .. ::.::*.**::**:***  *:

S.pombe          GIIKFFGKISSLLETNGVLILEPQGWDSYLKAAKKISVFNQTPENLKIQPDAFEHLLNQA    226
H.sapiens        GLKRMFRRIYRHLRPGGILVLEPQPWSSYGKRKTLTETIYKNYYRIQLKPEQFSSYLTSP    243
D.melanogaster   GLKMAFKRMFNQLRPGGKLILEAQNWASYKKKKNLTPEIYNNYKQIEFFPNKFHEYLLSS    298
                 *:   * ::   *. .* *:** * * ** *  .    : :.  .::: *: *   * .

S.pombe          GLVLEYSIEPQVNNSEYKNFAKRTMYIYKKKGIGI-        261
H.sapiens        DVGFSSYELVATPHNTSKGFQ-RPVYLFHKARSPSH        278
D.melanogaster   EVGFSHSYTLGVPRHMNKGFC-RPIQLYAKGDYTPN        333
                  : :.      . .   *.*  * : :: *
```

C

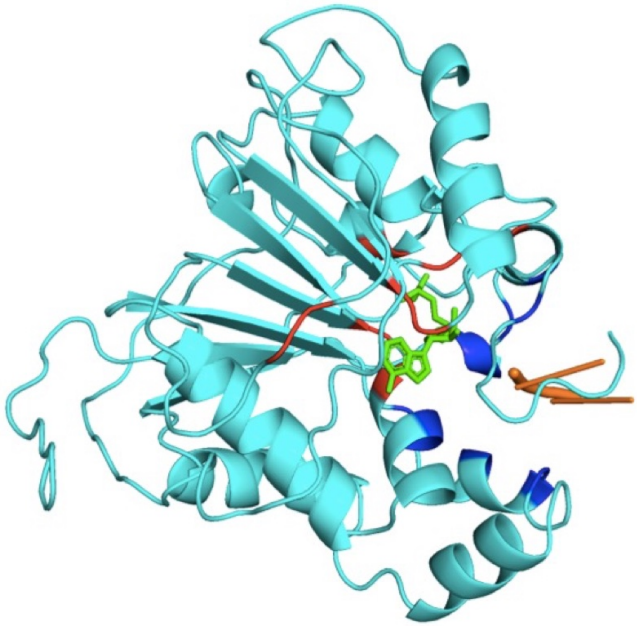

Supplementary figure 1: Bin3 is the *S. pombe* methyl phosphate capping enzyme (MePCE) homolog

A) Schematic of the domain architecture of Bin3 homologs from *S. pombe*, *H. sapiens,* and *D. melanogaster*.

B) Clustal alignment of the methyltransferase/SAM-binding domains of *S. pombe* Bin3, *H. sapiens* MePCE, and *D. melanogaster* Bin3. Predicted SAM-binding residues are indicated in red and nucleotide-binding residues are in blue.

C) Phyre2 structure prediction 67 of *S. pombe* Bin3 bound to a 5' terminal guanosine (orange) and SAH (green). Predicted SAM-binding residues are in red and nucleotide-binding residues are in blue.

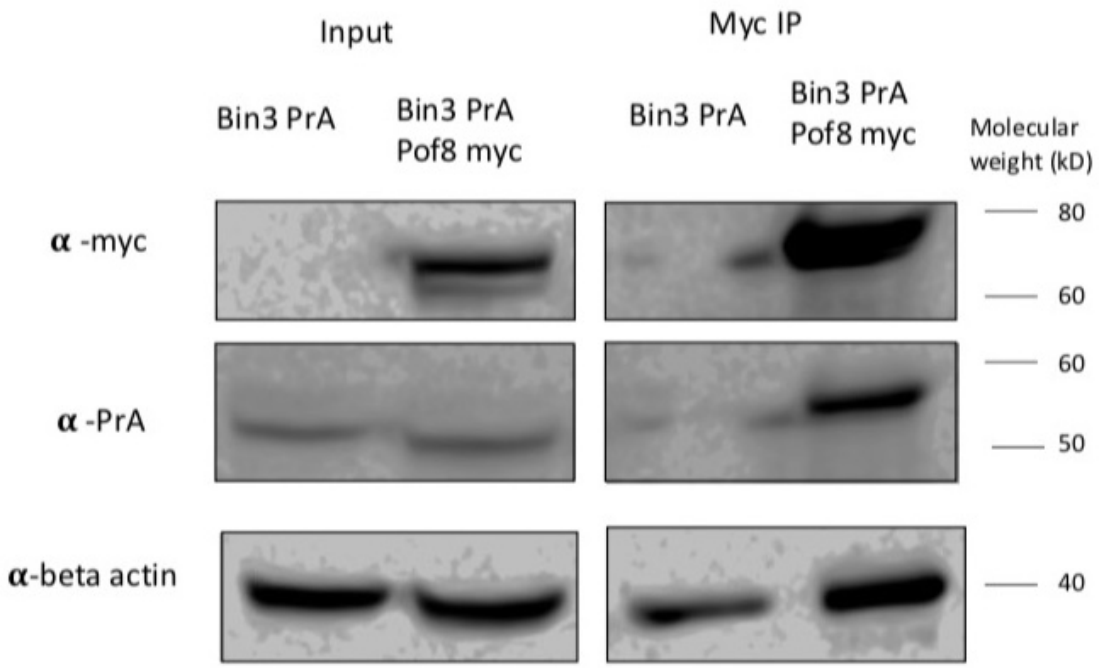

Supplementary figure 2: Reciprocal co-immunoprecipitations validate an interaction between Bin3 and Pof8

The interaction between Bin3 and Pof8 was confirmed by a-myc co-immunoprecipitation.

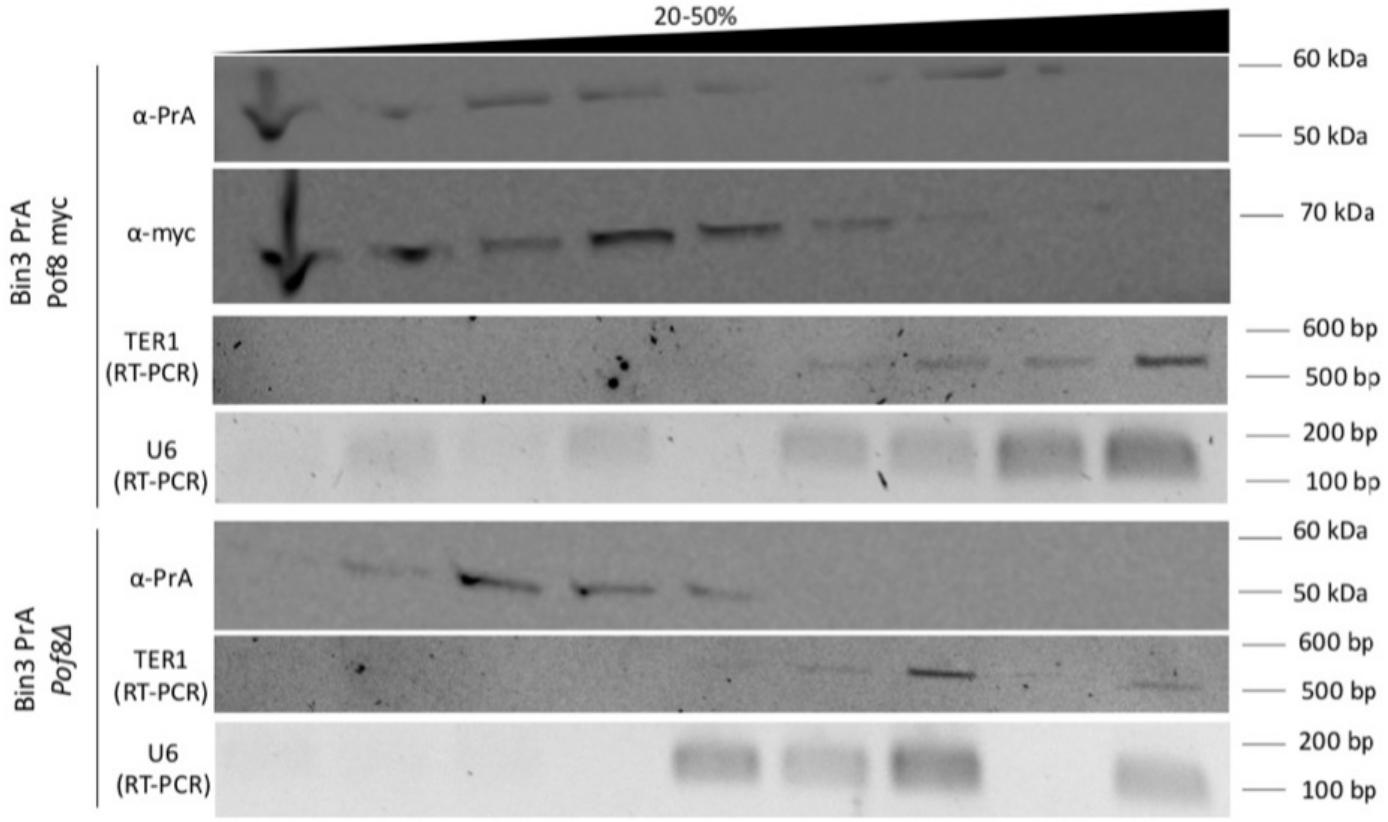

Supplementary figure 3: Glycerol gradient sedimentation of Bin3, Pof8, TER1, and U6 in a wild type and pof8Δ strain

Western blot and semi-quantitative RT-PCR of Bin3 PrA, Pof8 myc, TER1, and U6 in gradient fractions.

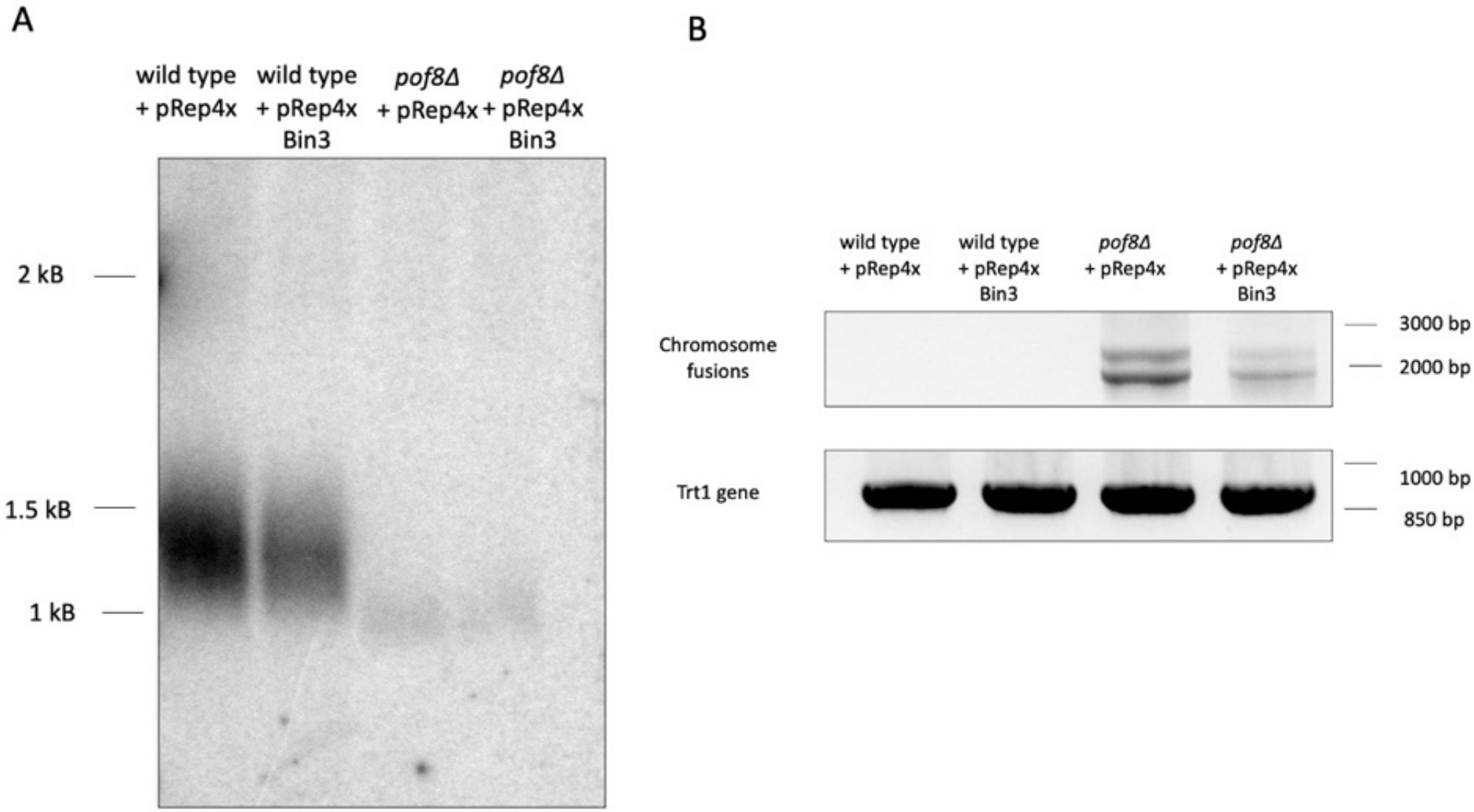

Supplementary figure 4: Bin3 overexpression fails to rescue *pof8Δ*-dependent telomere defects

A) Chromosome fusion PCR (top) following 2 restreaks on minimal media (one re-streak= 20-25 generations) from wild type and *pof8Δ* strains overexpressing an empty vector (pRep4x) or Bin3. The Trt1 gene was amplified from genomic DNA as a loading control (bottom).

B) Southern blot comparing telomere length from the same genomic DNA as (A). Genomic DNA was digested with EcoRI.

A

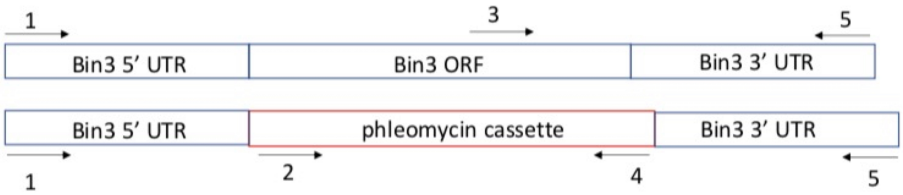

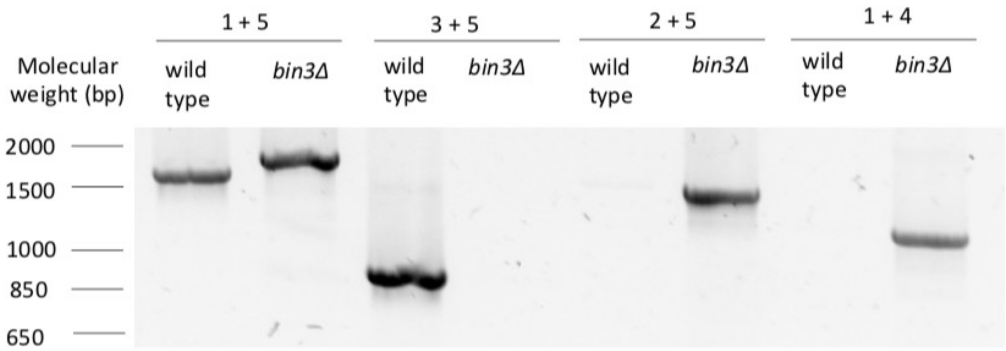

B

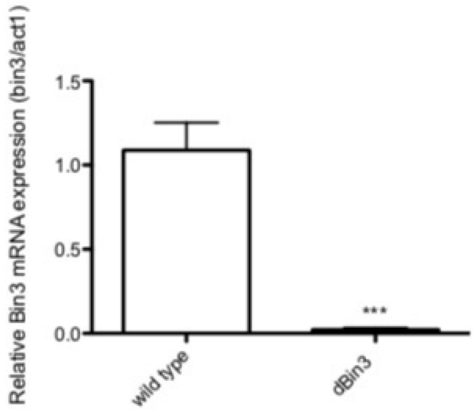

C

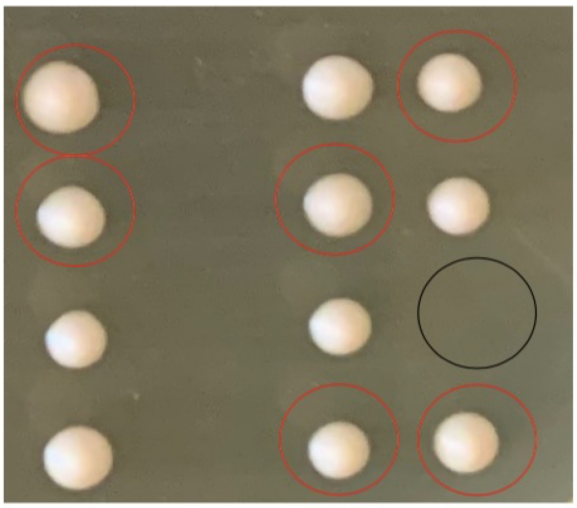

D

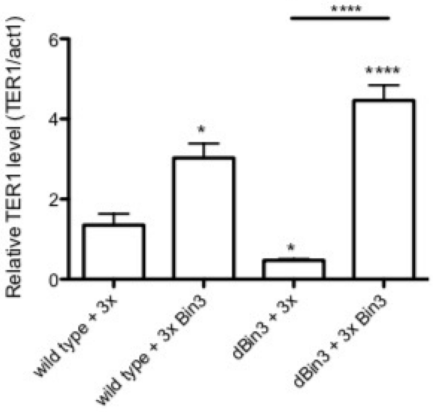

Supplementary figure 5: Validation of a Bin3 knockout strain confirms its viability

A) Schematic of Bin3 knockout (top) and PCR validation of the resultant strain using the indicated primers.
B) qRT-PCR of bin3 mRNA normalized to act1 mRNA for wild type and bin3Δ strains (mean ± standard error, paired t test * at $p < 0.05$, ** at $p < 0.01$, *** at $p < 0.001$, and **** at $p<0.0001$) (n=3 biological replicates). P-values over each bar represent results of a paired t-test with a wild type strain.
C) Backcrossing of bin3Δ and a wild type strain, followed by tetrad dissection, confirms viability of the bin3Δ strain on rich media. Tetrads from the same spore are arranged in columns. Resulting haploid colonies possessing phleomycin resistance are circled in red and colonies that didn't grow after tetrad dissection are circled in black.
D) qRT-PCR of TER1 normalized to act1 mRNA for wild type and bin3Δ strains transformed with an empty vector (3x) or Bin3 (mean ± standard error, paired t test * at $p < 0.05$, ** at $p < 0.01$, *** at $p < 0.001$, and **** at $p<0.0001$) (n=3 biological replicates). P-values over each bar represent results of a paired t-test with a wild type strain transformed with an empty vector (wild type + pRep3x).

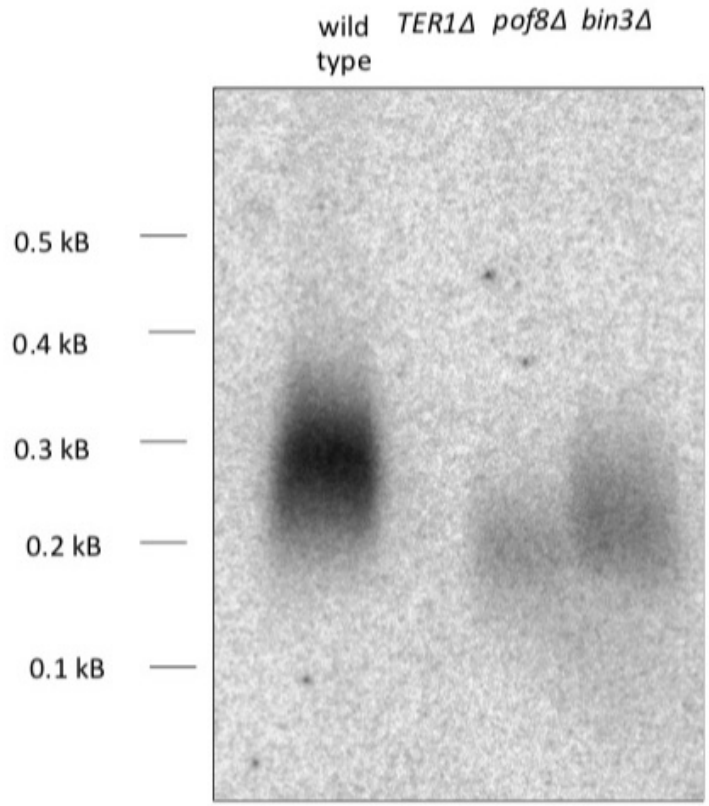

Supplementary figure 6: Bin3 and Pof8 are not strictly required for telomere maintenance

Southern blot comparing ApaI-digested genomic DNA isolated after 5 restreaks on rich media. A lack of signal with a telomeric probe represents survivors that have lost telomeric DNA and circularized their chromosomes (*TER1Δ*).

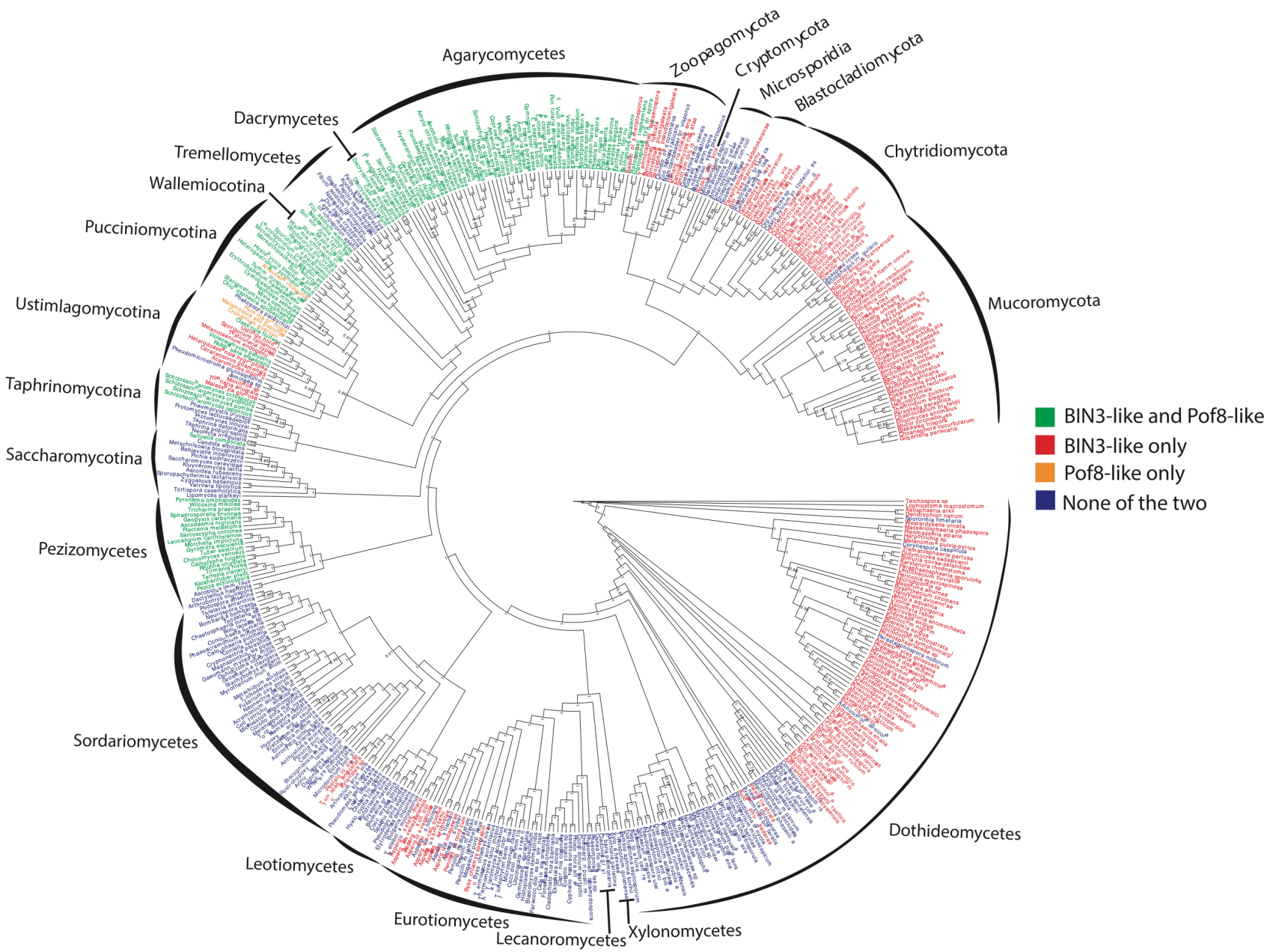

Supplementary figure 7: Phylogenic distribution of Bin3 and Pof8 in fungi
Complete consensus cladogram describing the phylogenic relationships of 472 species representative of fungi phylum and classes and highlighting (using a color code) the distribution of Bin3 and Pof8 in these species. Only posterior probabilities inferior to 1 are shown.